Available online at www.sciencedirect.com
ScienceDirect
International Journal of Plasticity 24 (2008) 1277–1306
INTERNATIONAL JOURNAL OF Plasticity
www.elsevier.com/locate/ijplas

# Interfacial gradient plasticity governs scale-dependent yield strength and strain hardening rates in micro/nano structured metals

Rashid K. Abu Al-Rub *

*Zachry Department of Civil Engineering, Texas A&M University, College Station, TX 77843, USA*

Received 22 June 2007; received in final revised form 13 September 2007
Available online 26 September 2007

**Abstract**

The effect of the material microstructural interfaces increases as the surface-to-volume ratio increases. It is shown in this work that interfacial effects have a profound impact on the scale-dependent yield strength and strain hardening of micro/nano-systems even under uniform stressing. This is achieved by adopting a higher-order gradient-dependent plasticity theory [Abu Al-Rub, R.K., Voyiadjis, G.Z., Bammann, D.J., 2007. A thermodynamic based higher-order gradient theory for size dependent plasticity. Int. J. Solids Struct. 44, 2888–2923] that enforces microscopic boundary conditions at interfaces and free surfaces. Those nonstandard boundary conditions relate a micro-traction stress to the interfacial energy at the interface. In addition to the nonlocal yield condition for the material's bulk, a microscopic yield condition for the interface is presented, which determines the stress at which the interface begins to deform plastically and harden. Hence, two material length scales are incorporated: one for the bulk and the other for the interface. Different expressions for the interfacial energy are investigated. The effect of the interfacial yield strength and interfacial hardening are studied by analytically solving a one-dimensional Hall–Petch-type size effect problem. It is found that when assuming compliant interfaces the interface properties control both the material's global yield strength and rates of strain hardening such that the interfacial strength controls the global yield strength whereas the interfacial hardening controls both the global yield strength and strain hardening rates. On the other hand, when assuming a stiff interface, the bulk length scale controls both the global yield strength and strain hardening rates. Moreover, it is found that in order to correctly predict the increase in the yield strength with decreasing size, the interfacial length scale should scale the magnitude of both the interfacial yield strength and interfacial hardening.


* Tel.: +1 979 862 6603; fax: +1 979 845 6554.
*E-mail address:* rabualrub@civil.tamu.edu

0749-6419/$ - see front matter © 2007 Elsevier Ltd. All rights reserved.
doi:10.1016/j.ijplas.2007.09.005

*Keywords:* Interfacial energy; Nonlocal; Size effect; Thin films; Length scale

## 1. Introduction

The emerging areas of micro and nanotechnologies exhibit important strength differences that result from continuous modification of the material microstructural characteristics with changing size, whereby the smaller is the size the stronger is the response. For example, experimental works have shown increase in strength by decreasing: (a) the particle size of particle-reinforced composites while keeping the volume fraction constant (e.g. Lloyd, 1994; Rhee et al., 1994; Zhu and Zbib, 1995; Nan and Clarke, 1996; Kiser et al., 1996); (b) the diameter of micro-wires under torsion (Fleck et al., 1994) [note that this experiment has not been repeated until now]; (c) the thickness of thin films under bending or uniaxial tension (e.g. Stolken and Evans, 1998; Huang and Spaepen, 2000; Shrotriya et al., 2003; Haque and Saif, 2003; Espinosa et al., 2004; Simons et al., 2006); (c) the indentation depth in micro/nano-indentation tests (e.g. Stelmashenko et al., 1993; DeGuzman et al., 1993; Ma and Clarke, 1995; Poole et al., 1996; McElhaney et al., 1998; Lim and Chaudhri, 1999; Elmustafa and Stone, 2002; Swadener et al., 2002) [note that there is a huge number of experimental results in the literature on this type of size effect but, surprisingly, very limited theoretical predictions]; (d) the grain size of nano-crystalline materials (the well-known Hall–Petch effect); the void size in nano-porous media; and several others.

Therefore, accurate identification of the mechanical properties of micro/nano-systems (e.g. micro/nano thin films, micro/nano wires, micro/nano-composites) is essential for the design, performance, and development of, for example, micro/nano electronics and micro/nanoelectromechanical systems (MEMS/NEMS) to be used, for example, as actuators or sensors (e.g. pressure, inertial, thermal, and chemical sensors, position detectors, accelerometers, magnetometers, micromirrors, etc.). The mechanical properties of small-scale structures are different from those of the conventional or bulk counterparts because they are very sensitive to the microstructural features of the material such as the grain size, the finite number of grains, the boundary layer thickness, texture, and dislocation structure. Therefore, when one or more of the dimensions of these systems begin to approach that of their microstructural features, the material mechanical properties (e.g. yield strength, strain hardening, fracture toughness) begin to exhibit a dependence on the structure size as schematically shown in Fig. 1. In metallic systems this translates to plastic yielding occurring at increased stresses over their bulk counterparts. The small sizes involved limit the conventional operation of dislocations and the application of classical continuum mechanics concepts; thus, a fundamental question arises: since the initial yield stress (i.e. onset of plasticity) in micro/nano-systems is size-dependent, a question that needs to be addressed, what yield strength should be used in the design of these systems?

Size effects in micro/nano-systems could not be explained by the classical continuum mechanics since no length scale enters the constitutive description (Fleck et al., 1994). A multiscale continuum theory, therefore, is needed to bridge the gap between the classical continuum theories and micromechanical theories. Since the increase in strength with decreasing scale can be related to proportional increase in the strain gradients (Aifantis,

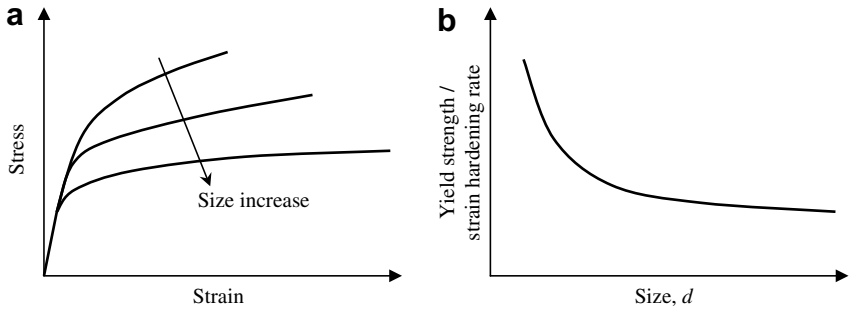


Fig. 1. Illustration of strengthening in micro/nano-systems. (a) Stress–strain diagrams for various sizes, and (b) increase in the yield strength and/or the rate of strain hardening as size decreases.

1984), which accommodate the evolution of geometrically necessary dislocations (GNDs) (Ashby, 1970), the gradient plasticity theory has been successful in addressing the size effect problem [see Voyiadjis and Abu Al-Rub (2005) for an extensive review of successful examples]. This success stems out from the incorporation of a microstructural length scale parameter through functional dependencies on the plastic strain gradient of nonlocal media. Furthermore, for mathematical consistency, in the gradient-dependent framework, additional boundary conditions have to be specified at interfaces and free surfaces allowing one to include interfacial effects which are the main focus of this paper.

However, recently many researchers who are engaged in nano/micro characterization have questioned the ability of the gradient plasticity theory in predicting the Hall–Petch-like size effect; i.e. the increase in the yield strength with decreasing the grain size under macroscopically homogeneous stressing or straining (i.e. under uniaxial tension or compression) (e.g. Uchic et al., 2004; Espinosa et al., 2004; Dimiduk et al., 2005; Greer et al., 2005; Volkert and Lilleodden, 2006; Simons et al., 2006). To the author's best knowledge this is attributed to lack of the physical understanding of the nature of the non-classical boundary conditions that the gradient plasticity theory enforces at the material free surfaces and interfaces. Free surfaces and interfaces of a material confined in a small volume can strongly affect the mechanical properties of the material. Free surfaces in submicron and nano-systems can be sources for development of defects and its propagation towards the interior. Hard, soft, or intermediate interfaces between distinct phase regions can also be locations for dislocations' blocking and pile-ups that give rise to strain gradients to accommodate the GNDs. The increase in the initial yield stress with decreasing thickness observed in tensile tests of various thin films (e.g. Huang and Spaepen, 2000; Haque and Saif, 2003; Espinosa et al., 2004) in the size range of 100–500 nm may be taken as a hint in this direction. The free surfaces of the thin film and the interface between the film and substrate, therefore, can have a significant effect on the strength of the thin film. Lower-order strain gradient plasticity theories (e.g. Gao et al., 1999; Acharya and Bassani, 2000; Gao and Huang, 2001; Abu Al-Rub and Voyiadjis, 2006) which neglect the application of the corresponding higher-order boundary conditions at interfaces and free surfaces indeed fail to predict boundary layer effects. Therefore, the focus of this paper is laid on the effect of dimensional constraints on the yield strength and plastic flow and to show that higher-order gradient plasticity theories (as opposed to lower-order theories) can be used

successfully to interpret size effects under macroscopically homogeneous stressing or straining conditions.

Dislocation pile-ups, which result in local plastic strain gradients, could be encountered at free surfaces and interface depending on the level of surface/interfacial energy which increases as the surface-to-volume ratio increases. In other words, it is expected that as the characteristic size decreases, the higher is the surface/interfacial energy and the more significant is the effect of the boundary layer thickness on the strength of the system. Therefore, size effect can be explained by constrained plastic slipping due to grain boundaries and interfaces which result in a nonuniform straining, thereby setting up strong gradients of strain. Plastic deformation in small-scale structures, accommodated by dislocation nucleation and movement, is therefore strongly affected by interfaces. Until now, little attention is devoted to interfacial strengthening effects (e.g. film–substrate interface, phase or grain boundaries, inclusion's interface, void free surface, nano-wires free surfaces, etc) on the scale-dependent plasticity in small-scale systems. Interface and boundary conditions for higher-order variables are generally modeled as infinitely stiff or completely free (e.g. see Nicola et al., 2003; von Blanckenhagen et al., 2004; Anand et al., 2005; Balint et al., 2005; Espinosa et al., 2006; Benzerga and Shaver, 2006; and the references quoted therein). These conditions are very difficult to be satisfied in reality, particularly, for systems with large surface-to-volume ratios. However, recently there have been few attempts to model intermediate (i.e. not free and not stiff) boundary conditions for higher-order variables within the higher-order strain gradient plasticity framework [see the works of Gurtin (2000, 2002), Gudmundson (2004), Fredriksson and Gudmundson (2005, 2007), Aifantis and Willis (2005, 2006), Aifantis et al. (2006), Abu Al-Rub et al. (2007)].

In this paper, the higher-order gradient plasticity theory, which has recently been developed by Abu Al-Rub et al. (2007) based on the principle of virtual power and the nonlocal Clausius–Duhem inequality, is used to investigate the size effect on the yield strength (i.e. onset of plasticity) and the flow stress (i.e. rates of strain hardening) by examining different forms for the interfacial energy at the interface of a micro/nano structured materials. However, it should be emphasized that one can perform the same analysis by using any other form of the numerous gradient plasticity theories that are available in the literature. Therefore, the conclusions that are drawn from using Abu Al-Rub et al. (2007) gradient theory are valid for all other gradient plasticity theories when those augmented by higher-order microscopic boundary conditions and relate them to the interfacial energy of the form presented in this paper. It is shown in the present paper that interfacial strengthening effects can be characterized within the strain gradient plasticity theory by incorporating an interfacial energy term in the internal power that depends on the plastic strain state at the interface of the plastically deforming material. Hence, two material length scales are incorporated: one for the bulk material and one for the interface, which together control the size effect at the micro- and nano-levels.

The reminder of this paper is organized as follows: In Section 2, the higher-order gradient plasticity theory of Abu Al-Rub et al. (2007) is recalled. The relation between the interfacial energy and the formulated higher-order boundary conditions is presented in Section 3. Application of the proposed framework for investigating the role of interfacial energy effect on the yield strength and flow stress of small-scale structures is presented in Section 4. Summary and conclusions are outlined in Section 5.

## 2. Thermodynamics of higher-order gradient plasticity

In order to be able to model the small-scale phenomena, such as the effect of size of microstructural features on the material mechanical properties, the higher-order strain gradient plasticity theory of Abu Al-Rub et al. (2007) is recapitulated. For tensors, index notation and the summation convention will be used. A comma followed by an index denotes differentiation with respect to a coordinate. Furthermore, the rectangular coordinates $x_k$ are employed here and a superimposed dot indicates the derivative with respect to time.

Small strain/small rotation plasticity and rate-independent material response is assumed here. The classical theory of isotropic plastic solids undergoing small deformations is based on the additive decomposition of the total strain-rate, $\dot{\boldsymbol{\varepsilon}}$, into an elastic part, $\dot{\boldsymbol{\varepsilon}}^{\mathrm{e}}$, and a plastic part, $\dot{\boldsymbol{\varepsilon}}^{\mathrm{p}}$:

$$\dot{\varepsilon}_{ij} = \dot{\varepsilon}^{\mathrm{e}}_{ij} + \dot{\varepsilon}^{\mathrm{p}}_{ij} \tag{1}$$

In classical continuum plasticity, $\dot{p}$ is defined as the rate of the local effective plastic strain, which is intended to measure the statistically stored dislocation (SSD) density and is expressed by

$$\dot{p} = \|\dot{\varepsilon}^{\mathrm{p}}_{ij}\| = \sqrt{\dot{\varepsilon}^{\mathrm{p}}_{ij}\dot{\varepsilon}^{\mathrm{p}}_{ij}} \tag{2}$$

while the unit direction of the plastic strain tensor, $\mathbf{N}$, is defined as follows:

$$N_{ij} = \dot{\varepsilon}^{\mathrm{p}}_{ij}/\|\dot{\varepsilon}^{\mathrm{p}}_{ij}\| = \dot{\varepsilon}^{\mathrm{p}}_{ij}/\dot{p} \;\Rightarrow\; \dot{\varepsilon}^{\mathrm{p}}_{ij} = \dot{p}N_{ij} \;\Rightarrow\; \dot{p} = \dot{\varepsilon}^{\mathrm{p}}_{ij}N_{ij} \tag{3}$$

where Eq. $(3)_2$ characterizes the classical (local) plasticity flow rule. One can also write the following useful relation by taking the gradient of Eq. (2), such that

$$\dot{p}_{,k} = \frac{\dot{\varepsilon}^{\mathrm{p}}_{ij}\dot{\varepsilon}^{\mathrm{p}}_{ij,k}}{\sqrt{\dot{\varepsilon}^{\mathrm{p}}_{mn}\dot{\varepsilon}^{\mathrm{p}}_{mn}}} = \frac{\dot{\varepsilon}^{\mathrm{p}}_{ij}}{\dot{p}}\dot{\varepsilon}^{\mathrm{p}}_{ij,k} = N_{ij}\dot{\varepsilon}^{\mathrm{p}}_{ij,k} \tag{4}$$

where $\dot{\varepsilon}^{\mathrm{p}}_{ij,k} = \nabla\dot{\boldsymbol{\varepsilon}}^{\mathrm{p}}$ is the gradient of the plastic strain tensor.

Based on the crystallographic analysis presented by Abu Al-Rub et al. (2007), it is concluded that one should consider the effects of both the gradient of the plastic strain tensor, $\nabla\boldsymbol{\varepsilon}^{\mathrm{p}}$, and the gradient of the effective plastic strain, $\nabla p$, in the development of scale-dependent plasticity such that one cannot exist without the other. Hence, the author believes that for a complete constitutive description at small length scales, the internal power and the Helmholtz free energy should not include only the effects of $\dot{\boldsymbol{\varepsilon}}^{\mathrm{p}}$ and $\dot{p}$ but should also include the effects of $\nabla\dot{\boldsymbol{\varepsilon}}^{\mathrm{p}}$ and $\nabla\dot{p}$. Although these variables may have a common origin in dislocation storage and motion, they will be treated here independent of each other. This gives different physical interpretations that guide one to different evolution equations and allowing one to computationally introduce the influence of one scale on the other (e.g. the effect of mesoscale on macroscale). For example dislocation interactions are observed on a mesolevel with length scale 0.1–10 μm affecting strongly the material behavior on the macrolevel with length scale $\geqslant 100$ μm. However, those variables are considered here mathematically related to their local counterparts and, therefore, special care must be taken to properly account for their coupling.

### 2.1. Principle of virtual power

The principle of virtual power is the assertion that, given any sub-body $\Gamma$, the virtual power expended on $\Gamma$ by materials or bodies exterior to $\Gamma$ (i.e. external power) be equal to the virtual power expended within $\Gamma$ (i.e. internal power). Let $\mathbf{n}$ denote the outward unit normal to $\partial\Gamma$. The external expenditure of power is assumed to arise from a macroscopic surface traction $t$, the microtraction stress tensor, $\mathbf{m}$, conjugate to $\dot{\boldsymbol{\varepsilon}}^{\mathrm{p}}$, defined for each unit vector $\mathbf{n}$ normal to the boundary $\partial\Gamma$ of $\Gamma$. Therefore, by neglecting body forces, one can write the external virtual power in the following form:

$$P_{\mathrm{ext}} = \int_{\partial\Gamma} (t_i\,\delta v_i + m_{ij}\,\delta\dot{\varepsilon}^{\mathrm{p}}_{ij})\mathrm{d}A \tag{5}$$

where $\mathbf{v}$ is the velocity vector. The kinematical fields $\delta\mathbf{v}$, $\delta\dot{\boldsymbol{\varepsilon}}^{\mathrm{p}}$, and $\delta\dot{p}$ in the above equation and the subsequent equations are considered as virtual, where $\delta$ is the variation parameter.

The external power is balanced by an internal expenditure of power characterized by the Cauchy stress tensor $\boldsymbol{\sigma}$ defined over $\Gamma$, the backstress $\mathbf{X}$ conjugate to $\boldsymbol{\varepsilon}^{\mathrm{p}}$ and associated with kinematic hardening, and the drag-stress $R$ conjugate to $p$ and associated with isotropic hardening. However, since the goal of this paper is a theory that incorporates the gradients of the plastic strain, one also considers power expenditures associated with kinematic variables $\nabla\boldsymbol{\varepsilon}^{\mathrm{p}}$ and $\nabla p$. One, therefore, can assume that additional power is expended internally by the higher-order microstress $\mathbf{S}$ conjugate to $\nabla\boldsymbol{\varepsilon}^{\mathrm{p}}$ and the higher-order microforce vector $\mathbf{Q}$ conjugate to $\nabla p$. Specifically, the internal virtual power is assumed to have the following form

$$P_{\mathrm{int}} = \int_{\Gamma} (\sigma_{ij}\,\delta\dot{\varepsilon}^{\mathrm{e}}_{ij} + X_{ij}\,\delta\dot{\varepsilon}^{\mathrm{p}}_{ij} + R\,\delta\dot{p} + S_{ijk}\,\delta\dot{\varepsilon}^{\mathrm{p}}_{ij,k} + Q_k\,\delta\dot{p}_{,k})\mathrm{d}V \tag{6}$$

and to balance $P_{\mathrm{ext}}$, Eq. (5), in the sense that $P_{\mathrm{ext}} = P_{\mathrm{int}}$.

It is noteworthy that one might argue that the energetic balance in Eqs. (5) and (6) might best be characterized through a dependence of $P_{\mathrm{int}}$ on the (scalar) accumulation of the plastic strain $p$ (internal history variable) and not on the plastic strain itself $\boldsymbol{\varepsilon}^{\mathrm{p}}$. However, the effects of the two variables are different: a dependence of $P_{\mathrm{int}}$ on $\boldsymbol{\varepsilon}^{\mathrm{p}}$ gives rise to kinematic hardening; while a dependence of $P_{\mathrm{int}}$ on $p$ gives rise to isotropic hardening (Gurtin, 2003). For example, in the Prager's hardening model (linear kinematic hardening) (Prager, 1956), the backstress is proportional to $\boldsymbol{\varepsilon}^{\mathrm{p}}$. However, a more general flux tensor associated with back-stress may be assumed (e.g. Scheidler and Wright, 2001; Voyiadjis et al., 2004; Clayton et al., 2006).

Substituting Eqs. (1), $(3)_3$, and (4) into the internal virtual power in Eq. (6) and then applying the divergence theorem yields, after some lengthy manipulations, the following result

$$\begin{aligned} P_{\mathrm{int}} = &-\int_{\Gamma} \sigma_{ij,j}\delta v_i\,\mathrm{d}V - \int_{\Gamma} [\tau_{ij} - X_{ij} + S_{ijk,k} + Q_k N_{ij,k} - (R - Q_{k,k})N_{ij}]\delta\dot{\varepsilon}^{\mathrm{p}}_{ij}\,\mathrm{d}V \\ &+ \int_{\Gamma} (R\dot{\varepsilon}^{\mathrm{p}}_{ij} + Q_k\dot{\varepsilon}^{\mathrm{p}}_{ij,k})\delta N_{ij}\,\mathrm{d}V + \int_{\partial\Gamma} \sigma_{ij}n_j\delta v_i\mathrm{d}A + \int_{\partial\Gamma} [S_{ijk} + Q_k N_{ij}]n_k\delta\dot{\varepsilon}^{\mathrm{p}}_{ij}\mathrm{d}A \end{aligned} \tag{7}$$

where $\tau$ is the deviatoric part of $\boldsymbol{\sigma}$ (i.e. $\tau_{ij} = \sigma_{ij} - \sigma_{kk}\delta_{ij}/3$).

Substituting Eqs. (5) and (7) into the virtual power balance, $P_{\mathrm{ext}} = P_{\mathrm{int}}$, and arranging terms, yields the following result

$$\int_{\Gamma}\sigma_{ij,j}\delta v_i\,\mathrm{d}V+\int_{\partial\Gamma}(t_i-\sigma_{ij}n_j)\delta v_i\,\mathrm{d}A+\int_{\Gamma}[\tau_{ij}-X_{ij}+S_{ijk,k}-(R-Q_{k,k})N_{ij}]\delta\dot{\varepsilon}^{\mathrm{p}}_{ij}\,\mathrm{d}V$$
$$+\int_{\partial\Gamma}[m_{ij}-(S_{ijk}+Q_kN_{ij})n_k]\delta\dot{\varepsilon}^{\mathrm{p}}_{ij}\,\mathrm{d}A=0 \tag{8}$$

The fields $\Gamma$, $\delta\mathbf{v}$, and $\delta\dot{\boldsymbol{\varepsilon}}^{\mathrm{p}}$ may be arbitrarily specified if and only if

$$\sigma_{ij,j}=0,\quad t_i=\sigma_{ij}n_j \tag{9}$$
$$\tau_{ij}-X_{ij}+S_{ijk,k}-(R-Q_{k,k})N_{ij}=0,\quad m_{ij}=(S_{ijk}+Q_kN_{ij})n_k \tag{10}$$

According to the notion of Gurtin (2003), Eq. $(9)_1$ expresses the local *macroforce balance*, Eq. $(9)_2$ defines the stress vector as the surface density of the forces imposes which also provides the local *macrotraction boundary conditions* on forces, Eq. $(10)_1$ is the nonlocal *microforce balance* detailed in the next subsection, and Eq. $(10)_2$ is the nonlocal *microtraction condition*, which is a higher-order internal boundary condition augmented by the interaction of dislocations across interfaces. The microtraction condition, Eq. $(10)_2$, is the soul of this paper as presented in Section 3.

### 2.2. Nonlocal plasticity yield surface

One can view the *microforce balance* in Eq. $(10)_1$ as the plasticity nonlocal yield condition. By taking the Euclidean norm $\|\|$ of Eq. $(10)_1$, the nonlocal plasticity loading surface $f$ can then be expressed as

$$f=\|\tau_{ij}-X_{ij}+S_{ijk,k}\|-R+Q_{k,k}=0 \tag{11}$$

where $\|R-Q_{k,k}\|=R-Q_{k,k}$ and $\|\mathbf{N}\|=1$. Furthermore, in obtaining Eq. (11), the associative plasticity flow rule and normality to the yield surface, similar to the local flow rule in Eq. $(3)_2$, is assumed which implies that $\mathbf{N}$ is collinear with $\boldsymbol{\tau}-\mathbf{X}+\mathrm{div}\,\mathbf{S}$. It is obvious that Eq. (11) represents a sphere in deviatoric stress-space of radius $R-\mathrm{div}\,\mathbf{Q}$ centered at $\mathbf{X}-\mathrm{div}\,\mathbf{S}$. One can notice that the higher-order stress div $\mathbf{S}$ is a backstress quantity giving rise to additional kinematic hardening, while the microstress div $\mathbf{Q}$ is giving rise to additional isotropic hardening (i.e. strengthening). One can also notice form Eq. (11) that in the absence of plastic strain gradients, the classical von-Mises yield criterion is recovered.

### 2.3. Application of the nonlocal Clausius–Duhem inequality

A thermodynamic procedure similar to the one advanced by Abu Al-Rub et al. (2007) is briefly pursued here.

Utilizing the derived microforce balance, Eq. $(10)_1$, and the microtraction condition, Eq. $(10)_2$, into the above equation, and replacing the virtual quantities by the actual fields, one can rewrite the expression of the internal power defined in Eq. (7) as follows:

$$P_{\mathrm{int}}=\int_{\Gamma}\sigma_{ij}\dot{\varepsilon}_{ij}\,\mathrm{d}V+\int_{\partial\Gamma}m_{ij}\dot{\varepsilon}^{\mathrm{p}}_{ij}\,\mathrm{d}A \tag{12}$$

Comparing the above equation with its corresponding local expression (i.e. $P_{\mathrm{int}}=\int_{\Gamma}\sigma_{ij}\dot{\varepsilon}_{ij}\,\mathrm{d}V$), implies that the long-range (nonlocal) energy interactions can be of non-vanishing within the material's bulk and interfaces, which is represented by the second term, $\int_{\partial\Gamma}m_{ij}\dot{\varepsilon}^{\mathrm{p}}_{ij}\,\mathrm{d}A$. Hence, according to the notion of Edelen and Laws (1971) and Eringen

and Edelen (1972), the energy term $\int_{\partial\Gamma} m_{ij}\dot{\varepsilon}^{\mathrm{p}}_{ij}\,\mathrm{d}A$ is called the *nonlocality energy residual*. Therefore, one can define the density of the nonlocality energy residual, $\mathbb{R}$, as follows:

$$\int_{\Gamma} \mathbb{R}\,\mathrm{d}V = \int_{\partial\Gamma} m_{ij}\dot{\varepsilon}^{\mathrm{p}}_{ij}\,\mathrm{d}A \tag{13}$$

where $\mathbb{R}$ results from microstructural interactions between the material points in the active plastic zone within the bulk and at interfaces. Substituting Eq. $(10)_2$ into Eq. (13) and then applying the divergence theorem gives $\mathbb{R}$ as

$$\mathbb{R} = S_{ijk,k}\dot{\varepsilon}^{\mathrm{p}}_{ij} + S_{ijk}\dot{\varepsilon}^{\mathrm{p}}_{ij,k} + Q_{k,k}\dot{p} + Q_k\dot{p}_{,k} \tag{14}$$

which shows that in the absence of plastic strain gradients, $\mathbb{R} = 0$.

However, in the absence of material interfaces (e.g. grain boundaries) and interfacial energies, Edelen and Laws (1971) and Eringen and Edelen (1972) (see also Polizzotto and Borino, 1998; Polizzotto, 2003) assumed that the nonlocality energy residual is equal to zero (i.e. $\int_{\Gamma} \mathbb{R}\,\mathrm{d}V = 0$) and called it the *insulation condition* meaning that the nonlocal energy is not allowed to flow from any point within the bulk to the outside of the interface. This means that dislocations are either allowed to escape through the material free surfaces (i.e. $\mathbf{m} = \mathbf{0}$) or blocked completely at the interface (i.e. $\dot{\varepsilon}^{\mathrm{p(I)}}_{ij} = \mathbf{0}$, where $\dot{\varepsilon}^{\mathrm{p(I)}}_{ij}$ is the plastic strain-rate at the interface). Thus, the interior surface energy that results from dislocation interactions at the surface/interface boundaries is neglected. According to the notion of Gurtin (e.g. Gurtin, 2000, 2002, 2003), satisfying the insulation condition implies either a micro-free boundary condition imposed at external free surfaces or a micro-clamped boundary condition imposed on the internal boundaries. However, those null boundary conditions of a microscopically rigid interface or a microscopically free surface are very difficult to be satisfied in reality, particularly, for large surface-to-volume ratios. Therefore, in order to take into account the effect of surface/interfacial energy, the global nonlocal energy residual should be non-vanishing (i.e. $\int_{\Gamma} \mathbb{R}\,\mathrm{d}V \neq 0$). Thus, $\mathbf{m}$ in the subsequent equations is meant to be the driving force at the material internal and external boundaries such that for an intermediate (i.e. not free and not clamped) kind of microscopic boundary condition, one has $\mathbf{m} \neq \mathbf{0}$ on $\partial\Gamma_{\mathrm{ext}}$ and $\dot{\boldsymbol{\varepsilon}}^{\mathrm{p(I)}} \neq \mathbf{0}$ on $\partial\Gamma_{\mathrm{int}}$, where $\partial\,\Gamma = \partial\Gamma_{\mathrm{int}} \cup \partial\Gamma_{\mathrm{ext}}$. Therefore, the microtraction stress $\mathbf{m}$ can be interpreted as the *interfacial stress* at interfaces which is conjugate to the interfacial plastic strain, $\varepsilon^{\mathrm{p(I)}}_{ij}$. One can, therefore, express the total strain energy stored at the interface in terms of the global nonlocality residual, $\int_{\Gamma} \mathbb{R}\,\mathrm{d}V$, as follows:

$$\int_{\partial\Gamma} \dot{\varphi}\,\mathrm{d}A = \int_{\Gamma} \mathbb{R}\,\mathrm{d}V = \int_{\partial\Gamma} m_{ij}\dot{\varepsilon}^{\mathrm{p}}_{ij}\,\mathrm{d}A \geqslant 0 \tag{15}$$

where $\varphi$ is the interfacial energy at interfaces and free surfaces.

Assuming isothermal conditions for simplicity and from the free energy inequality (i.e. the rate of change in the total free energy should be less than or equal to the power done by external forces), one can write

$$\int_{\Gamma} \rho\dot{\Psi}\,\mathrm{d}V \leqslant P_{\mathrm{ext}} \tag{16}$$

where $\Psi$ is the specific free energy and $\rho$ is the material density. By substituting Eqs. (12) and (13) into Eq. (16), one obtains the following thermodynamic restriction in a point wise format

$$\sigma_{ij}\dot{\varepsilon}_{ij} - \rho\dot{\Psi} + \mathbb{R} \geqslant 0 \tag{17}$$

The inequality in Eq. (17) is termed as the *nonlocal Clausius–Duhem inequality* differing from its classical counterpart only in the presence of $\mathbb{R}$. This inequality holds everywhere in $\Gamma$, but $\mathbb{R} = 0$ at material points in the elastic zone. Moreover, it can be noticed that for a homogeneous plastic strain distribution $\mathbb{R} = 0$ such that the classical Clausius–Duhem inequality is retained.

It is noteworthy from the above arguments that in a point wise the density of the nonlocal energy residual, $\mathbb{R}$, is energy in the plastic bulk and on plastic interfaces, whereas globally the nonlocal energy residual, $\int_\Gamma \mathbb{R}\,\mathrm{d}V$, is energy on plastic interfaces and not in the bulk since the insulation condition requires that no energy exchanges occur between the material points within the same bulk. For example, for polycrystalline materials, $\int_\Gamma \mathbb{R}\,\mathrm{d}V = 0$ within the plastic bulk of each grain and $\int_\Gamma \mathbb{R}\,\mathrm{d}V \neq 0$ at the grains boundaries which are plastically deformed. For more details, the reader is referred to Abu Al-Rub et al. (2007).

Assuming a separable material, i.e. no coupling between the elastic and plastic free energies (Gurtin, 2000, 2002, 2003), one can write the Helmholtz free energy potential as

$$\Psi = \Psi^e(\varepsilon^{\mathrm{e}}_{ij}) + \Psi^{\mathrm{p}}(\varepsilon^{\mathrm{p}}_{ij}, p, \varepsilon^{\mathrm{p}}_{ij,k}, p_{,k}) \tag{18}$$

On expanding the time derivative of Eq. (18) and substituting the result into Eq. (17) along the use of Eqs. (1) and (14), one obtains the following thermodynamic state laws:

$$\sigma_{ij} = \rho\frac{\partial\Psi^e}{\partial\varepsilon^{\mathrm{e}}_{ij}}, \quad X_{ij} = \rho\frac{\partial\Psi^{\mathrm{p}}}{\partial\varepsilon^{\mathrm{p}}_{ij}}, \quad R = \sigma_{\mathrm{y}} + \rho\frac{\partial\Psi^{\mathrm{p}}}{\partial p}, \quad S_{ijk} = \rho\frac{\partial\Psi^{\mathrm{p}}}{\partial\varepsilon^{\mathrm{p}}_{ij,k}}, \quad Q_k = \rho\frac{\partial\Psi^{\mathrm{p}}}{\partial p_{,k}} \tag{19}$$

where $\sigma_{\mathrm{y}}$ is the scale-independent yield strength. Note that in obtaining Eqs. $(19)_2$ and $(19)_3$ it is assumed that $\mathbf{X} = \rho\Psi^{\mathrm{p}}/\boldsymbol{\varepsilon}^{\mathrm{p}}$ and $R - \sigma_{\mathrm{y}} = \rho\,\partial\Psi^{\mathrm{p}}/\partial p$ such that $\mathbf{X} = \mathbf{0}$ and $R = \sigma_{\mathrm{y}}$ at initial yielding. For more details, the reader is referred to Abu Al-Rub et al. (2007).

In order to develop equations amenable to the analysis and computation, one now considers a simple example for the definition of the Helmholtz free energy function. Both $\Psi^e$ and $\Psi^{\mathrm{p}}$ that appear in Eq. (18) can be assumed to have, respectively, the following analytical forms:

$$\rho\Psi^e = \frac{1}{2}\varepsilon^{\mathrm{e}}_{ij}E_{ijkl}\varepsilon^{\mathrm{e}}_{kl}, \quad \rho\Psi^{\mathrm{p}} = \frac{h}{m+2}\left(\frac{e}{\varepsilon_{\mathrm{y}}}\right)^{m+2}\varepsilon_{\mathrm{y}}^2 + \frac{1}{2}a\left(\varepsilon^{\mathrm{p}}_{ij}\varepsilon^{\mathrm{p}}_{ij} + \ell^2\varepsilon^{\mathrm{p}}_{ij,k}\varepsilon^{\mathrm{p}}_{ij,k}\right) \tag{20}$$

where $\mathbf{E}$ is the symmetric fourth-order elastic stiffness tensor, $h$, $m > 0$, and $a$ are material constants, and $\varepsilon_{\mathrm{y}}$ is the yield strain. The parameter $e$ is the generalized total accumulation of plastic strain and plastic strain gradients that is intended to measure the total dislocation density (SSDs and GNDs) (see e.g. Fleck et al., 1994; Gurtin, 2003; Gudmundson, 2004; Abu Al-Rub and Voyiadjis, 2004a), which is defined by

$$e^2 = p^2 + \ell^2 p_{,k}p_{,k} \tag{21}$$

where $\ell$ is the bulk material length scale parameter used for dimensional consistency. In spite of the crucial importance of $\ell$ in the gradient theory, very limited work is focused on the physical origin of this length scale parameter. The discrete dislocation origin of $\ell$ is rarely clear and its value is usually a free parameter. However, initial attempts have been made to relate $\ell$ to the microstructure of the material. Nix and Gao (1998) identified $\ell$ as $L^2/b$, where $L$ is the average spacing between dislocations, and $b$ is the magnitude of the

Burgers vector. Moreover, based on the Taylor's hardening law, an expression for $\ell$ in terms of macroscopic and microscopic quantities was derived as (e.g. Nix and Gao, 1998; Abu Al-Rub and Voyiadjis, 2004a; Abu Al-Rub, 2007):

$$\ell = 18\alpha^2 \left(G/\sigma_y\right)^2 b \tag{22}$$

where $\alpha$ is an empirical parameter (ranges from 0.1 to 0.3) and $G$ is the shear modulus. However, Abu Al-Rub and Voyiadjis (2004a, 2006) and Voyiadjis and Abu Al-Rub (2005) have shown that this length scale is not fixed but depends on the mean free path of dislocations such that it evolves with the course of plastic deformation. Abu Al-Rub and Voyiadjis (2004b) also derived an evolution equation for $\ell$ as a function of temperature, strain, strain-rate, and a set of measurable microstructural physical parameters. In this work, this length scale is assumed to be constant for simplicity. However, the accurate quantitative predictions of the gradient plasticity theory hinges on one's ability to determine accurate values for $\ell$ from non-traditional tests (e.g. micro/nano-indentation, micro-torsion, micro-bending). For more details about the physical interpretation of $\ell$, its relationship to the material's microstructural features, and its identification from micro/nano-indentation tests, the reader is referred to Abu Al-Rub and Voyiadjis (2004a,b) and Abu Al-Rub (2007).

Making use of Eqs. (20) into Eqs. (19), the following laws are obtained:

$$\sigma_{ij} = E_{ijkl}(\varepsilon_{kl} - \varepsilon^{\mathrm{p}}_{kl}), \quad X_{ij} = a\varepsilon^{\mathrm{p}}_{ij}, \quad R = \sigma_y + h(e/\varepsilon_y)^m p \tag{23}$$

$$S_{ijk} = a\ell^2 \varepsilon^{\mathrm{p}}_{ij,k}, \quad Q_k = h\ell^2 (e/\varepsilon_y)^m p_{,k} \tag{24}$$

Substituting the above equations into the nonlocal yield function $f$, Eq. (11), then one can write

$$f = \|\tau_{ij} - a\varepsilon^{\mathrm{p}}_{ij} + a\ell^2 \nabla^2 \varepsilon^{\mathrm{p}}_{ij}\| - \sigma_y - h(e/\varepsilon_y)^m p + h\ell^2 \frac{\partial}{\partial x_k}[(e/\varepsilon_y)^m p_{,k}] = 0 \tag{25}$$

where $\nabla^2$ designates the Laplacian operator. In the absence of plastic strain gradients, the classical von-Mises criterion is retrieved. Furthermore, by setting $a = m = 0$, one obtains the gradient plasticity yield function of Aifantis (1984). Furthermore, the combinations $a\ell^2$ and $h\ell^2$ control the flow stress enhancement provided by the plastic strain gradients.

It should be emphasized that the nonlocal yield function in Eq. (25) should be supplemented by the microscopic boundary conditions derived in Eq. $(10)_2$. Therefore, the description is not complete until the physical nature of the higher-order boundary conditions is specified. This is achieved next.

## 3. Interfacial effects

In this section, the interface micromechanics is modeled within the presented higher-order gradient plasticity framework. Plastic deformation is mainly carried by dislocations within the bulk (e.g. individual grains). Dislocations can move through the crystal grains and can interact with each other. Interfaces (e.g. grain boundaries) often hinder their transmission, creating a dislocation pile-up at the interface and thereby making the material harder to deform. Therefore, plastic deformation is strongly affected by interfaces. It will be shown here that the microscopic boundary conditions in Eq. $(10)_2$ is related to the interfacial energy at free surfaces (e.g. the surface of a freestanding thin film, the free

surface of a void) or interfaces (e.g. the film–substrate interface, grain boundaries, inclusion interface). This interfacial energy introduces an interfacial resistance against dislocation emission/transmission.

Interfacial energy in small-scale systems (e.g. thin films, nano wires, nano-composites, nano-crystalline material) is significant and cannot be ignored when the surface-to-volume ratio becomes large enough. For submicron and nano length scales the surface-to-volume ratio is appreciable. In Eq. $(10)_2$, the microtraction stress $\mathbf{m}$ is meant to be the driving force at the material internal and external boundaries, which can be interpreted as the *interfacial stress* at free surface or interface which is conjugate to the surface plastic strain. Therefore, $\mathbf{m}$ can be related to the interfacial energy $\varphi$ per unit surface area by using the well-known relation (see Gurtin and Murdoch, 1978):

$$m_{ij} = \frac{\partial \varphi(\boldsymbol{\varepsilon}^{\mathrm{p}})}{\partial \varepsilon_{ij}^{\mathrm{p(I)}}} \quad \text{on } \partial \Gamma^{\mathrm{p}} \tag{26}$$

where $\boldsymbol{\varepsilon}^{\mathrm{p(I)}}$ is the plastic strain at the interface and $\partial \Gamma^{\mathrm{p}}$ is the plastic interface. Continuity of the strain field requires $\boldsymbol{\varepsilon}^{\mathrm{p}}|_{\partial\ \Gamma^{\mathrm{p}}} = \boldsymbol{\varepsilon}^{\mathrm{p(I)}}$ at the interface. Therefore, $\varepsilon^{\mathrm{p(I)}}$ and the bulk plastic strain $\boldsymbol{\varepsilon}^{\mathrm{p}}$ are identical at the interface. The components of $\boldsymbol{\varepsilon}^{\mathrm{p(I)}}$ are the extensional and shear plastic strains with respect to a locally rectangular coordinate system defined in the tangent plane of the interface at the material point of interest. However, it may be argued that the plastic strain should vanish at an elastic–plastic boundary. As explained in Fredriksson and Gudmundson (2007), the interfacial region has a finite but small thickness such that the plastic strain varies within this thickness and vanishes at the border between the interfacial region and the elastic material. However, if the thickness of the interfacial region is neglected, then the interface can be modeled as a mathematical surface where jumps in the plastic strain are allowed. Moreover, since the accumulation of dislocations at the interface corresponds to a misorientation angle $\theta$, one can physically interpret, for small deformations, the plastic shear strain on the plastically deforming side of the interface as the misorientation angle $\theta$ (Read and Shockley, 1950).

According to the definition in Eq. (26), $\varphi = 0$ designates a free surface where dislocations are allowed to escape, while $\varphi \to \infty$ designates a micro-clamped surface (i.e. rigid interface) where dislocations are not allowed to penetrate. Hence, constrained plastic flow could be modeled either as a full constraint, i.e. $\boldsymbol{\varepsilon}^{\mathrm{p}} = 0$ (when $\varphi \to \infty$), or no constraint, i.e. $\mathbf{m} = 0$ (when $\varphi \to 0$). However, following the ideas presented by Gudmundson (2004), Fredriksson and Gudmundson (2005, 2007), Aifantis and Willis (2005, 2006), Aifantis et al. (2006), and Abu Al-Rub et al. (2007) an intermediate kind of micro-boundary condition is introduced. Therefore, the interfacial energy $\varphi$ presented in Eq. (26) can be assumed to have the following form in analogy with linearly hardening bulk materials:

$$\varphi = \gamma \left\| \varepsilon_{ij}^{\mathrm{p(I)}} \right\| + \frac{1}{2}\beta \left\| \varepsilon_{ij}^{\mathrm{p(I)}} \right\|^2 \quad \text{on } \partial \Gamma^{\mathrm{p}} \tag{27}$$

where $\|\varepsilon_{ij}^{\mathrm{p(I)}}\| = \sqrt{\varepsilon_{ij}^{\mathrm{p(I)}} \varepsilon_{ij}^{\mathrm{p(I)}}}$ is a measure of the plastic strain accumulation at the interface, $\gamma$ is the interfacial yield strength which characterizes the stiffness of the interface boundary in blocking dislocations from crossing the interface, and $\beta$ is an interfacial property which characterizes the interfacial hardening that results during the transference of dislocation pile-ups across the interface. Therefore, both $\gamma$ and $\beta$ are interfacial properties. If $\gamma = 0$, the interface would yield at the same time as the bulk yields and consequently interfacial effect is controlled by the interfacial hardening parameter $\beta$. Whereas, if $\beta = 0$, the interface

would yield at a different time as the bulk yields, but the interface does not harden. The role of both $\gamma$ and $\beta$ on the qualitative behavior of size effect is thoroughly examined in the next section.

The microtraction stress at the boundary, $\mathbf{m}$, can then be obtained from Eqs. (26) and (27) as

$$m_{ij} = \gamma \frac{\varepsilon_{ij}^{\mathrm{p(I)}}}{\left\| \varepsilon_{mn}^{\mathrm{p(I)}} \right\|} + \beta \varepsilon_{ij}^{\mathrm{p(I)}} \quad \text{on } \partial \Gamma^{\mathrm{p}} \tag{28}$$

such that for $\boldsymbol{\varepsilon}^{\mathrm{p(I)}} = 0$, $m_{ij} = \pm \gamma \delta_{ij}$. The microtraction stress is thus collinear with the plastic strain at the interface.

Physically, as argued by Aifantis and Willis (2005), this corresponds to a yield-like condition at the interface, $f^{\mathrm{(I)}}$, similar to the yield condition for the bulk, $f$, such that one can assume the following expression for the interfacial yield condition:

$$f_{\mathrm{I}} = \|m_{ij}\| - \gamma - \beta p_{\mathrm{I}} = 0 \tag{29}$$

where $p_{\mathrm{I}} = \int_0^t \|\dot{\varepsilon}_{ij}^{\mathrm{p(I)}}\| \mathrm{d}t$. The above interfacial yield condition can be used to determine the stress at which the interface begins to deform plastically and hardens. This means that if $\|m_{ij}\| < \gamma$, then the interface is impenetrable to dislocations and no plastic deformation is developed at the interface. Once $\|m_{ij}\| = \gamma$, the interface yields plastically such that the plastic strain there is not zero, which implies that interfacial hardening is activated. Then the interface continues to deform as long as $\|m_{ij}\| \geqslant \gamma$ in a linear hardening mode characterized by the parameter $\beta$ such that plastic strain accumulates in both the interface and the bulk interior through dislocation motion and multiplication. Therefore, it follows from the above arguments that $\gamma$ is qualitatively analogous to $\sigma_{\mathrm{y}}$ and $\beta$ is analogous to $h$ in Eq. (25).

One can also assume that the interfacial strength, $\gamma$, scales with the bulk yield strength, $\sigma_{\mathrm{y}}$, and that the interfacial hardening, $\beta$, also scales with the bulk hardening modulus, $h$, by an interfacial length scale, $\ell_{\mathrm{I}}$, such that Eq. (29) can be rewritten as

$$f_{\mathrm{I}} = \|m_{ij}\| - \ell_{\mathrm{I}}(\sigma_{\mathrm{y}} + h p_{\mathrm{I}}) = 0 \tag{30}$$

where $\ell_{\mathrm{I}}$ is an another microstructural length scale parameter (besides the bulk length scale parameter $\ell$), which is related to the boundary layer thickness and defines the interface yield and hardening properties. The above proposition is supported by the undesirable behavior resulted from applying Eq. (29) as will be seen in the next section. Moreover, $\ell_{\mathrm{I}}$ sets the level of interfacial energy such that Eq. (30) ensures that if $\ell_{\mathrm{I}} = 0$, the interface would behave like a free surface and one obtains a micro-free boundary condition (i.e. $\mathbf{m} = 0$). On the other hand, if $\ell_{\mathrm{I}} \to \infty$ then it would represent a condition for fully constrained dislocation movement at the interface and one obtains a micro-clamped boundary condition (i.e. $\boldsymbol{\varepsilon}^{\mathrm{p(I)}} = 0$). This is consistent with the requirement that when $\varphi \to \infty$ then $\boldsymbol{\varepsilon}^{\mathrm{p(I)}} = 0$ and when $\varphi \to 0$ then $\mathbf{m} = 0$. Therefore, Eq. (30) may yield different strengthening behavior than Eq. (29) as shown in the coming section. Furthermore, in Eq. (30), the stiffness and hardening of the interface is altered simultaneously by the length scale $\ell_{\mathrm{I}}$, while in Eq. (29) the interfacial strength and hardening can be altered independently. In order to reveal the interesting features of the proposed model, the size effect behaviors obtained by using Eqs. (29) and (30) are examined in the next section for a simple analytical solution of a one-dimensional Hall–Petch-type size effect.

Concerning the physical nature of the interfacial length scale, $\ell_I$, more studies are needed to identify this issue. However, according to Read and Shockley (1950), the interfacial energy at grain boundaries can be expressed in terms of the misorientation (or misfit) angle $\theta$ such that for a low-angle tilt boundary, one can write

$$\varphi = \frac{Gb\theta}{4\pi(1-\nu)}\left(\log\frac{eb}{2\pi r_0} - \log\theta\right) \tag{31}$$

where $G$ is the shear modulus, $b$ is the magnitude of the Burgers vector, $\nu$ is Poisson's ratio, $r_0$ is the radius of the dislocation core, and $e$ is the base of the natural logarithm. For small deformations, $\theta$ can be interpreted as the interfacial plastic shear strain such that the interfacial effective plastic strain $p_I = \sqrt{\varepsilon_{ij}^{p(I)}\varepsilon_{ij}^{p(I)}}$ takes the value of $p_I = \theta/\sqrt{2}$. Therefore, substituting in Eq. (31) for $\theta$ the term $\sqrt{2}p_I$ and comparing the result to Eq. (27) with $\gamma = \ell_I\sigma_y$, one obtains after neglecting the nonlinear terms $\log\theta$ and $(p_I)^2$ the following expression for $\ell_I$ in terms of macroscopic and microscopic quantities:

$$\ell_I = \frac{\sqrt{2}}{4\pi(1-\nu)}\left(\frac{G}{\sigma_y}\right)b\log\left(\frac{eb}{2\pi r_0}\right) \tag{32}$$

If one sets $\nu = 0.3$, $G/\sigma_y = 100$, $b = 0.225$ nm, and $\log(eb/2\pi r_0) = 0.23$ (Read and Shockley, 1950), then $\ell_I = 0.83$ nm. If $\sigma_y = 100$ MPa, then the magnitude of the interfacial energy is $\gamma = \sigma_y\ell_I = 0.083$ N/m, which seems a very small value. Similarly, by substituting the above values into Eq. (22) with $\alpha = 0.3$, one obtains $\ell = 3.65$ μm, which is a physically sound value in the range of micrometers. However, it is not known to the author if the value of the interfacial length scale is in the correct order. Initial attempts are made here, but more studies are needed in this direction and for relating $\ell_I$ to the bulk length scale $\ell$. Moreover, although the concept of slip planes is smeared out in obtaining Eq. (32), the dislocation model and the present model can be compared qualitatively.

## 4. Application to the Hall–Petch-type size effect

This section presents an application of the formulated higher-order gradient plasticity model to handle size effects in small-scale structures under macroscopically uniform uniaxial stress. In order to discover all the qualitative aspects of the proposed interfacial properties, in the following, an analytical solution is formulated for problems involving one spatial dimension. For example, a single-phase bicrystal under tension or compression where the interface represents a grain boundary (see Fig. 2a), or a thin film on an elastic substrate under tension or compression (see Fig. 2b), or a thin film–substrate system or a single-phase bicrystal under simple shear loading. In all these cases, there is just one relevant component of stress, displacement, total strain, plastic strain, plastic strain gradient, and higher-order stresses. Therefore, it is appropriate to drop all suffixes, and to let $x$ denote the coordinate in which there is variation, $\sigma_0$ is the applied stress, and $d$ is the characteristic size of the specimen (e.g. the bicrystal grain size or the film thickness). From Fig. 2, the interface is positioned at $x = 0$ and the free surface is at $x = d$. For simplicity and in order to obtain a closed-form solution for the plastic strain, the material is taken to be uniform and linearly hardening elasto-plastic such that the exponent $m$ in Eq. (25) is set to zero.

It is noteworthy that the proposed higher-order gradient plasticity theory presented in the previous sections is directed towards polycrystals obeying a macroscopic plastic flow.

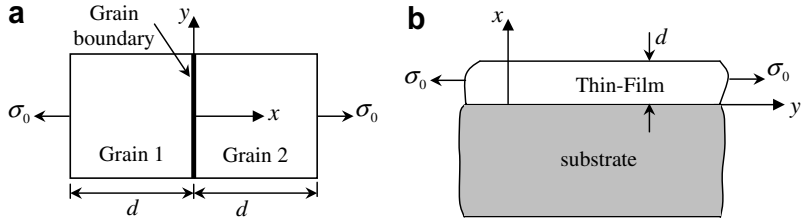


Fig. 2. One-dimensional model for (a) a thin film on an elastic substrate and (b) a single-phase bicrystal.

To realistically describe single crystals and bicrystals, a slip-system based formulation of crystal plasticity theory (e.g. Asaro, 1983) would seem more appropriate. This theory should account for the orientation of the lattice, misorientation across the boundary, and slip transmission/blockage across the interface (e.g. Zikry and Kao, 1996). However, although the concept of slip planes is smeared out in the present model, the crystal plasticity model and the present model can be compared qualitatively. Moreover, the following 1-D solution would still be applicable towards polycrystalline and nano-crystalline films and columnar structures.

According to the above realization, one can reduce the nonlocal yield condition in Eq. (25) to an ordinary differential equation for the plastic strain as follows:

$$\varepsilon^{\mathrm{p}}_{,xx} - \frac{1}{\ell^2}\varepsilon^{\mathrm{p}} = -\left(\frac{\sigma_0 - \sigma_{\mathrm{y}}}{h\ell^2}\right) \tag{33}$$

where $\varepsilon^{\mathrm{p}}_{,xx} = \partial^2\varepsilon^{\mathrm{p}}/\partial x^2$. Note that the applied stress $\sigma_0$ is uniform and satisfies the macro-force balance in Eq. $(9)_1$ such that $\partial\sigma_0/\partial x = 0$.

It is convenient to express the above equation in a non-dimensional form with the aid of variable substitution (i.e. $z = x/d$, $\bar{\varepsilon}^{\mathrm{p}} = \varepsilon^{\mathrm{p}}/\varepsilon_{\mathrm{y}}$, and $\bar{\sigma}_0 = \sigma_0/\sigma_{\mathrm{y}}$ with $\varepsilon_{\mathrm{y}} = \sigma_{\mathrm{y}}/E$ being the yield strain and $E$ is the Young's modulus) such that

$$\bar{\varepsilon}^{\mathrm{p}}_{,zz} - \lambda^2\bar{\varepsilon}^{\mathrm{p}} = -F \tag{34}$$

with constant coefficients $\lambda = d/\ell$ and $F = (\bar{\sigma}_0 - 1)/(h/E)(\ell/d)^2$.

It is assumed that the microtraction stress $\mathbf{m}$ in Eq. $(10)_2$ vanishes at the free surface (i.e. at $x = d$) such that from Eqs. $(10)_2$ and (24) with the exponent $m = 0$, the following micro-free boundary condition is obtained

$$\bar{\varepsilon}^{\mathrm{p}}_{,z} = 0 \quad \text{at } z = 1 \tag{35}$$

Now the microscopic boundary condition at the interface (i.e. at $x = 0$) is prescribed by making use of the interfacial energy effect as presented in the previous section. Eqs. (29) or (30) can be written after substituting Eqs. $(10)_2$ and (24) for $\mathbf{m}$ and normalizing the result as follows:

$$(\ell/d)\bar{\varepsilon}^{\mathrm{p}}_{,z} = (E/h)\delta_1 + \delta_2\bar{\varepsilon}^{\mathrm{p}} \quad \text{at } z = 0 \tag{36}$$

where $\delta_1 = \gamma/\sigma_{\mathrm{y}}\ell$ and $\delta_2 = \beta/h\ell$ characterize the non-dimensional interfacial strength and hardening, respectively. However, if Eq. (30) is used instead of Eq. (29), one can then simply set $\delta_1 = \delta_2 = \delta = \ell_1/\ell$.

Solving the ordinary differential equation, Eq. (34), which is subjected to the boundary conditions in Eqs. (35) and (36), one obtains a closed-form expression for $\bar{\varepsilon}^{\mathrm{p}}(z)$ as

$$\bar{\varepsilon}^{\mathrm{p}}(z) = \frac{F}{\lambda^2} - \left[\frac{(E/h)\delta_1 + (F/\lambda^2)\delta_2}{\sinh\lambda + \delta_2\cosh\lambda}\right]\cosh\lambda(1-z) \tag{37}$$

with $F/\lambda^2 = (E/h)(\bar{\sigma}_0 - 1)\mathrm{H}(\bar{\sigma}_0 - 1)$, where $\mathrm{H}(\bar{\sigma}_0 - 1)$ is the Heaviside step function which implies that $\varepsilon^{\mathrm{p}} = 0$ as long as $\sigma_o \leqslant \sigma_{\mathrm{y}}$. For $\delta_1 = \delta_2 = 0$, one obtains the classical solution $\bar{\varepsilon}^{\mathrm{p}} = F/\lambda^2$ which is uniform along $d$.

Substituting Eq. (37) back into the normalized expression of the stress–strain relationship (i.e. $\bar{\sigma}_0 = \bar{\varepsilon} - \bar{\varepsilon}^{\mathrm{p}}$), and then integrating the result for $z$ from 0 to 1, one finds an expression for the normalized average total strain, $\bar{\varepsilon}^{\mathrm{ave}}$, which can then be rearranged as follows:

$$\bar{\sigma}_0 = \frac{\bar{\varepsilon}^{\mathrm{ave}} + (E/h)[1 + (\delta_1 - \delta_2)/\{\lambda(1 + \delta_2\coth\lambda)\}]}{1 + (E/h)[1 - \delta_2/\{\lambda(1 + \delta_2\coth\lambda)\}]} \tag{38}$$

It is assumed here that $\bar{\varepsilon}^{\mathrm{ave}}$ is positive. Furthermore, if $\bar{\varepsilon}^{\mathrm{ave}} \leqslant \sigma_{\mathrm{y}}/E$, the plastic strain is zero and the applied stress is related to the average total strain such that $\bar{\sigma}_0 = \bar{\varepsilon}^{\mathrm{ave}}$.

Eqs. (37) and (38) can be plotted for different sizes, $\ell/d$, different interfacial strengths, $\delta_1$, and different interfacial hardenings, $\delta_2$. Results in Figs. 3–10 are presented for $h/E = 0.2$. Different sizes are represented by $\ell/d = 0.1$, 0.5, 1, 1.5, and 2. The level of interfacial energy at the interface is controlled by both the normalized interfacial yield strength parameter, $\delta_1$, and hardening parameter, $\delta_2$. Furthermore, results for setting $\delta_1 = \delta_2 = \delta = \ell_{\mathrm{I}}/\ell$, which corresponds to the proposition in Eq. (30), are also presented. Setting $\delta_1 = \delta_2 = \delta$ implies that both the interfacial yield strength and hardening are altered simultaneously for different values of $\delta$. Therefore, in the following, four different cases for the mathematical form of the interfacial energy, $\varphi$, are examined, which are

*Case* (1). $\varphi = \gamma\varepsilon^{\mathrm{p(I)}}$, which is equivalent to setting $\delta_2 = 0$ in Eqs. (36)–(38) and indicates that the interface is not allowed to harden.

*Case* (2). $\varphi = \frac{1}{2}\beta(\varepsilon^{\mathrm{p(I)}})^2$, which is equivalent to setting $\delta_1 = 0$ in Eqs. (36)–(38) and indicates that the interface deforms plastically (i.e. yields) at the same time the bulk interior yields, but it is allowed to harden differently.

*Case* (3). $\varphi = \gamma\varepsilon^{\mathrm{p(I)}} + \frac{1}{2}\beta(\varepsilon^{\mathrm{p(I)}})^2$ such that Eqs. (36)–(38) are used as they are, but assigning different values for $\delta_1$ and $\delta_2$ (i.e. $\delta_1 \neq \delta_2$). This characterizes both interfacial yielding and hardening analogous to the bulk interior.

*Case* (4). $\varphi = \ell_{\mathrm{I}}[\sigma_{\mathrm{y}}\varepsilon^{\mathrm{p(I)}} + \frac{1}{2}h(\varepsilon^{\mathrm{p(I)}})^2]$ which is equivalent to setting $\delta_1 = \delta_2 = \delta = \ell_{\mathrm{I}}/\ell$ in Eqs. (36)–(38). This is similar to Case (3) but both the interfacial yield strength and hardening are controlled by the boundary layer length scale $\ell_{\mathrm{I}}$.

The above four cases are examined in detail in the following subsections.

### 4.1. Influence of the interfacial yield strength – Case (1)

The influence of the interfacial yield strength, $\gamma$, separated from the effect of interfacial hardening, $\beta$, is examined first by varying the non-dimensional measure $\delta_1$ and setting

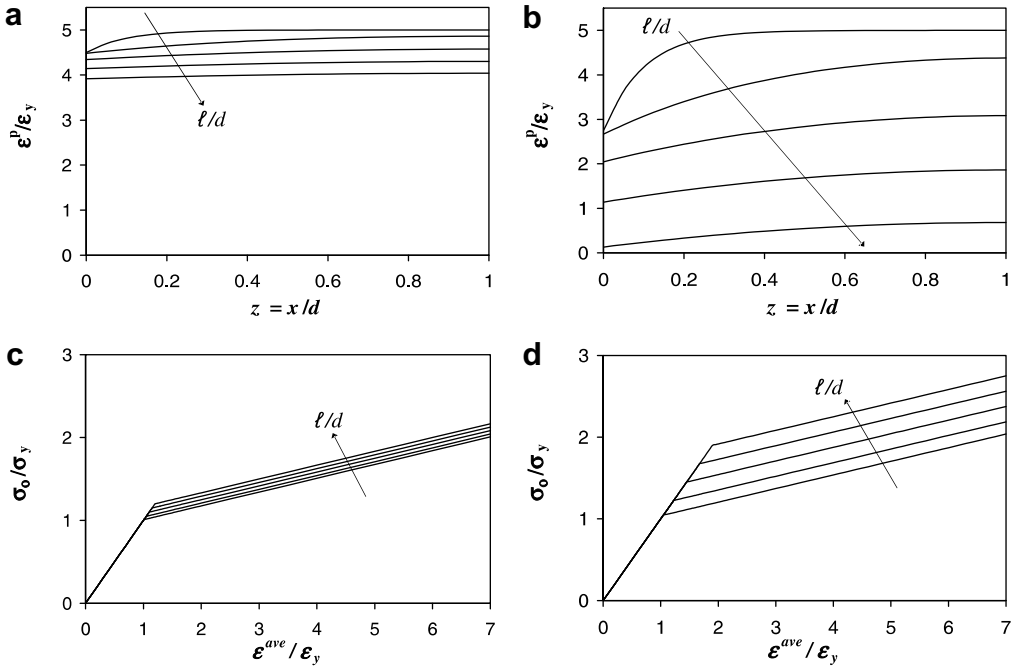


Fig. 3. Size effects due to interfacial yield strength only without interfacial hardening. The interfacial yield strength is varying according to [(a) and (c)] $\delta_1 = 0.1$ and [(b) and (d)] $\delta_1 = 0.45$. (a) and (b) normalized plastic strain distribution along $d$ for $\bar{\sigma}_0 = 2$. (c) and (d) normalized stress–strain relations. Different sizes are represented by $\ell/d = 0.1, 0.5, 1, 1.5, 2$.

$\delta_2 = 0$ in Eqs. (36)–(38). In Fig. 3, the effects of two values of $\delta_1$ on the distribution of plastic strain through the characteristic size $d$ at an applied stress of $\bar{\sigma}_0 = 2$ (Fig. 3a and b) and on the stress–strain relationship (Fig. 3c and d) are plotted for different ratios $\ell/d$ (if $\ell$is assumed constant, this is equivalent to varying the specimen size). Namely $\delta_1 = 0.1$ which corresponds to a compliant interface (i.e. interface with low yield strength) and $\delta_1 = 0.45$ corresponds to a stiff interface (i.e. interface with high yield strength). It is obvious from Fig. 3a and b that at $z = 0$ and for a specific $\ell/d$ the compliant interface deforms plastically much more than the stiff interface which results in a lower size effect as evidenced by Fig. 3c and d. Furthermore, the plastic strain distribution decreases as $d$ decreases or $\gamma$ increases, which in turn results in a higher flow stress (stress after the yield point) with decreasing $d$ or increasing $\gamma$.

Interestingly, Fig. 3c and d shows that the global yield strength (i.e. onset of plasticity) of the specimen is increased by increasing either $\delta_1$ or $\ell/d$ (or equivalently by increasing $\gamma$ or decreasing $d$ when $\ell$ is assumed constant). Following an initial elastic response, a yield point characterized by a deviation from the elastic response is seen with the yield strength increases as the size decreases (i.e. Hall–Petch effect). This is obvious for both values of $\delta_1$, but more for the stiff interface. Hence, it can be concluded that *the interfacial yield strength determines the specimen global yield strength*. It is also noted that the tangent hardening modulus after the yield point is constant and is not affected either by increasing $\delta_1$ or $\ell/d$. This is attributed to not allowing the interface to harden (i.e. setting $\delta_2 = 0$) as is

shown in the next subsection. Moreover, it is noteworthy that if the microscopic boundary conditions (equivalently the interfacial energy) effect is neglected, then no size effect of any kind could be obtained. Moreover, it is noted from Fig. 3a and c that even small variations in the plastic strain distribution can result in a pronounced size effect on the average stress–strain relationship.

One can obtain for this case (i.e. when the interfacial hardening is neglected) an expression for the yield strength in Fig. 3c and d (i.e. onset of plasticity in the bulk interior) as a function of the interfacial yield strength, $\gamma$, and size, $d$, by simply finding the value of the normalized applied stress at which the average plastic strain in the specimen is zero; that is $\bar{\sigma}_0 = \bar{\sigma}_Y$ when $(\bar{\varepsilon}^{\mathrm{p}})^{\mathrm{ave}} = 0$, where $\bar{\sigma}_Y$ is interpreted as the normalized global size-dependent yield strength of the whole specimen and $(\bar{\varepsilon}^{\mathrm{p}})^{\mathrm{ave}}$ is the average plastic strain in the specimen. This can be achieved simply by setting $\delta_2 = 0$ in Eq. (37), integrating the result over $z$, and substituting $\lambda = d/\ell$, which yields

$$\bar{\sigma}_Y = 1 + \delta_1(\ell/d) \tag{39}$$

which can be rewritten after substituting $\bar{\sigma}_Y = \sigma_Y/\sigma_{\mathrm{y}}$ and $\delta_1 = \gamma/\sigma_{\mathrm{y}}\ell$ as follows:

$$\sigma_Y = \sigma_{\mathrm{y}} + \gamma d^{-1} \tag{40}$$

This relation shows that the yield strength, $\sigma_Y$, scales with the interfacial yield strength, $\gamma$, and increases linearly with the inverse of the specimen size, $d^{-1}$ (note that $d$ could be interpreted here as the grain size, film thickness, or any characteristic dimension where there is variation in the plastic strain distribution).

It is noteworthy that Eq. (40) matches to a great extent the findings of some of the experimental and discrete dislocation studies of the dependence of the yield strength on the thickness of thin metal films. For example, the effects of grain size and film thickness on the yield strength were separated experimentally by Venkatraman and Bravman (1992). Those authors established an almost linear increase of yield strength with the inverse of both film thickness and grain size. Also, the calculations made by Nix (1989) of thin film plasticity with a single misfit dislocation proposed a linear dependence of the flow stress on the inverse of the film thickness.

The type of size effect in Eq. (40) can be referred to as *Orowan strengthening* ($\sigma_Y \propto d^{-1}$) that is analogous to the well-known *Hall–Petch strengthening* ($\sigma_Y \propto d^{-1/2}$), where the later states that the yield strength for polycrystalline materials increases linearly with the inverse of square root of the grain size, such that:

$$\sigma_Y = \sigma_{\mathrm{y}} + k_{\mathrm{HP}} d^{-1/2} \tag{41}$$

where $d$ is the mean grain size, $\sigma_{\mathrm{y}}$ is the yield strength of a single crystal, and $k_{\mathrm{HP}}$ is the Hall–Petch constant. Comparing Eqs. (40) and (41), one may conclude that $k_{\mathrm{HP}}$ may be related to the interfacial yield strength, $\gamma$. However, although the Hall–Petch law provides a realistic prediction for the yield strength of metallic polycrystals from large grain sizes down to 1 μm or less, the physical mechanisms underlying this size effect are still a matter of debate [see Lefebvre et al. (2007) and the references cited therein]. Moreover, until now, it is hardly possible to make a clear distinction between the Hall–Petch strengthening, Eq. (41), and the Orowan strengthening, Eq. (40), based on dislocation driven mechanisms.

It is noteworthy that there are many studies that have been conducted to explain the observed deviations in Eq. (41) for grain sizes less than 10 μm. Hirth (1972) proposed a model for grain size effect by modeling the polycrystal as a composite microstructure of

grain interior regions surrounded by hard grain boundary regions. Using this model with plastic incompatibility concepts (Ashby, 1970), Hirth (1972) obtained Eq. (40) (i.e. $\sigma_Y \propto d^{-1}$). Moreover, Borg (2007) fitted the increase in flow stress as a function of the grain size to a function in the form of $d^{-n}$ for different grain boundary energy parameters. Exponents, $n$, in the range 0.82–1.25 at initial yield and in the range 0.77–1.09 after 0.1 logarithmic strain are observed. These values are somewhat higher than what is predicted from the classical Hall–Petch relationship with exponent $n = 0.5$, but closer to that in Eq. (40), $n = 1$. In the study of Evers et al. (2004) using a scale-dependent model to predict grain size effects in a polycrystal under plane stress loading conditions, they found a Hall–Petch exponent in the range 1.19–1.50. Biner and Morris (2002) and Balint et al. (2005) used discrete dislocation plasticity models to analyze the dependence of shear yield strength on grain size, and observed Hall–Petch exponents in the range of 0.4–1.0. The reader is referred to Balint et al. (2007) for more details about the deviation of the Hall–Petch model in Eq. (41) and for an extensive review of the different models that are proposed in the literature in order to address this problem.

It is also worth mentioning that a possible source of the discrepancy between the Hall–Petch relation in Eq. (41) and that derived by the gradient plasticity theory, Eq. (40), is that the gradient plasticity relation is based on a formulation that assumes linear hardening, which is not allowed for in the Hall–Petch model. Therefore, by including nonlinear hardening (i.e. $m > 0$ in Eq. (25)) one may get a relation for the global yield strength from the gradient plasticity solution that closely resembles the Hall–Petch model. This will be shown in a future work through a finite element implementation of the proposed gradient-dependent theory. Moreover, considering both the interfacial yielding and interfacial hardening, which will be presented in Section 4.3, could change the behavior given by Eq. (40).

Now the question that needs an answer: what is the critical applied stress that is required to yield or plastically deform the interface? One may expect that this stress is higher than the global yield strength, Eq. (40), since the interfacial yield strength is expected to be higher than the yield strength of the bulk interior. This can be done by plotting the plastic strain at the interface (i.e. at $z = 0$) from Eq. (37) versus the applied stress. This is shown in Fig. 4a for different sizes and for the stiff interface (i.e. for $\delta_1 = 0.45$). As can be seen from this figure that as $d$ decreases, a higher stress is needed to plastically deform the interface. An expression for this critical stress, $\sigma_c$, can be obtained by setting the plastic strain at the interface in Eq. (37) to zero (i.e. $\bar{\varepsilon}^p(z = 0) = 0$) and solving for $\bar{\sigma}_0 = \bar{\sigma}_c$, which yields

$$\bar{\sigma}_c = 1 + \delta_1 / \tanh \lambda \tag{42}$$

The critical stress $\bar{\sigma}_c$ can also be interpreted as the stress corresponding to the onset of dislocation transfer across interfaces or dislocation emission takes place at interfaces and can also be referred to as *interfacial yield stress*. Hence, as long as the applied stress is less than the interfacial yield stress, the plastic strain at the interface is zero. After this critical stress is reached the interface deforms in a perfectly plastic manner, independently of both the interfacial plastic strain and the hardening of the bulk interior. Furthermore, it can be noted from Eq. (42) that if $\gamma = 0$, then the interface yields at the same time as the bulk interior. Therefore, it can be concluded that, in general, *the interface does not yield with the rest of the material, but follows its own yield behavior*.

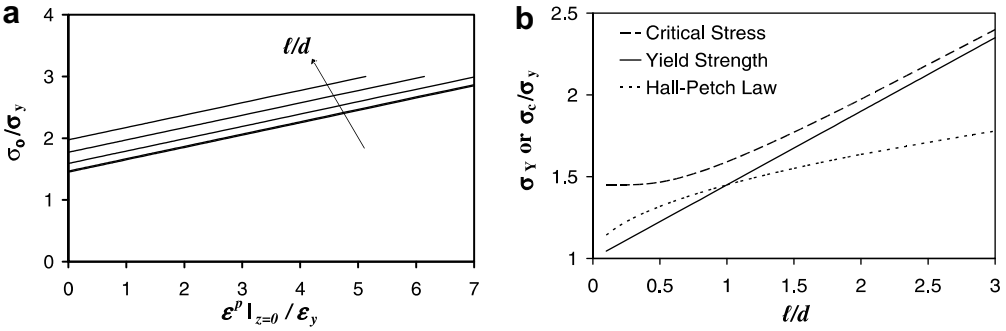


Fig. 4. (a) Plastic strain at the interface vs. the applied stress for different sizes represented by $\ell/d = 0.1$, 0.5, 1, 1.5, 2. (b) Variation of the global yield strength, $\sigma_Y$ in Eq. (39), the Hall–Petch relation, Eq. (41), and the critical stress necessary to yield the interface, $\sigma_c$ in Eq. (42), with size. The interfacial yield strength is represented by $\delta_1 = 0.45$.

Eq. (42) along with Eq. (39) are plotted in Fig. 4b for $\delta_1 = 0.45$. Furthermore, the normalized counterpart of the Hall–Petch relation in Eq. (41) is shown for comparison [$\sigma_Y = 1 + \delta_1 (\ell/d)^{-1/2}$, where $\delta_1 = k_{HP}/\sigma_y \ell^{-1/2}$]. It can be seen from Fig. 4b, as suggested before, that the bulk interior yields before the interface and as $d$ decreases, a higher stress is needed to plastically deform the interface. However, it is interesting to note that as $d$ decreases (or equivalently as $\ell/d$ increases) the difference between the global yield strength and the critical stress is decreasing. This implies that for very small $d$ (i.e. $\ell/d \to \infty$) the yield strength coincides with the critical stress (i.e. $\sigma_c = \sigma_Y$), which means that the bulk interior is vanishing and is replaced by the interface. This is particularly seen in ultrafine-grained metals where the grain boundaries occupy the majority of the volume, which implies that for those materials the interfacial yielding controls the global yield strength. Moreover, this interpretation is in good agreement with the observation that no dislocation is found inside the grains volume of ultrafine-grained polycrystals (Kumar et al., 2003). For nano-crystalline metals, the role played by bulk plasticity would be greatly diminished because dislocations seldom stay inside the bulk but are either absorbed into or piled up near the grain boundary. Correspondingly, the role of interfacial plasticity processes, as regulators of bulk dislocation fluxes and as carriers of plastic strain themselves, is markedly enhanced. On the other hand, for very large $d$ (i.e. $\ell/d \to 0$), the bulk interior yields much earlier than the interface such that the bulk yields at $\sigma_Y = \sigma_y$ whereas the interface yields at $\sigma_c = 1.45\sigma_y$. This can be interpreted as that the dislocations will take some time to reach the interface and pile-ups and then transfer across.

### 4.2. Influence of the interfacial hardening – Case (2)

It will now be assumed that the interface hardens (i.e. $\delta_2 \neq 0$), but yields at the same time as the bulk interior (i.e. $\delta_1 = 0$). In Fig. 5a–d, the plastic strain distribution and the average stress–strain relation are shown for two interface conditions; an intermediate interface with $\delta_2 = 1$ and a stiff interface with $\delta_2 = 10$. It can be seen from Fig. 5c and d that additional contribution to strain hardening that arises from the interaction of dislocations with the interface through interfacial hardening is noticed. This indicates that both

the tangent hardening modulus and flow stress are strongly affected by the interfacial hardening such that the tangent modulus increases as $d$ decreases when interfacial hardening is considered (i.e. $\delta_2 \neq 0$), and is independent of $d$ when interfacial hardening is neglected (i.e. $\delta_2 = 0$). An expression for the tangent hardening modulus, $E^{\mathrm{T}} = \mathrm{d}\sigma/\mathrm{d}\varepsilon$, normalized by the elastic modulus, $E$, can be obtained by taking the derivative of Eq. (38) with respect to $\bar{\varepsilon}^{\mathrm{ave}}$, such that:

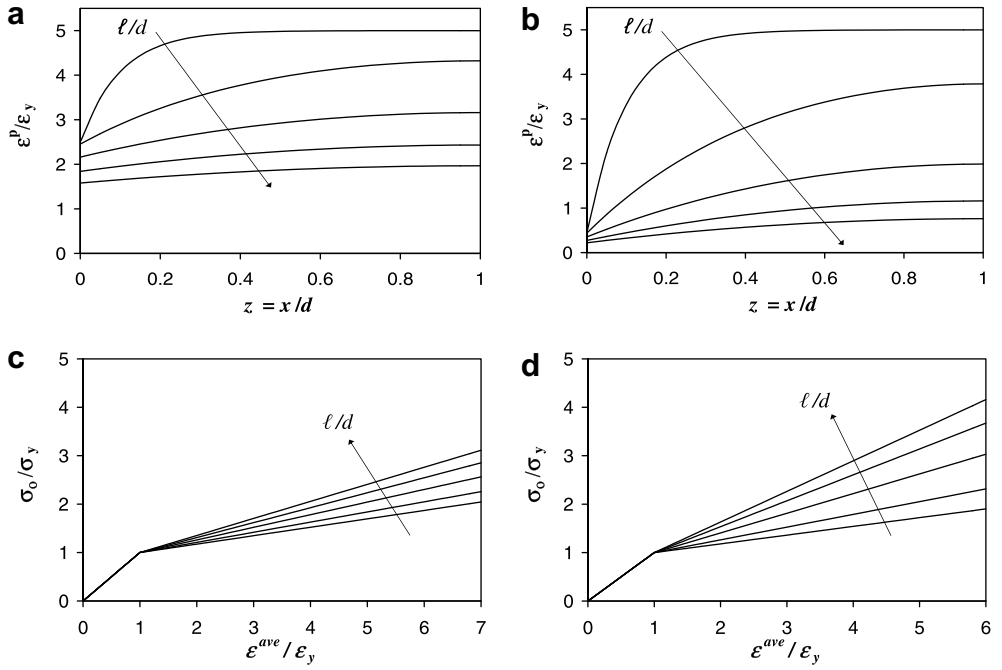


Fig. 5. Size effects due to interfacial hardening with a zero interfacial yield strength. The interfacial hardening is varying according to [(a) and (c)] $\delta_2 = 1$ and [(b) and (d)] $\delta_2 = 10$. (a) and (b) normalized plastic strain distribution along $d$ for $\bar{\sigma}_0 = 2$. (c) and (d) normalized stress–strain relations. Different sizes are represented by $\ell/d = 0.1$, 0.5, 1, 1.5, 2.

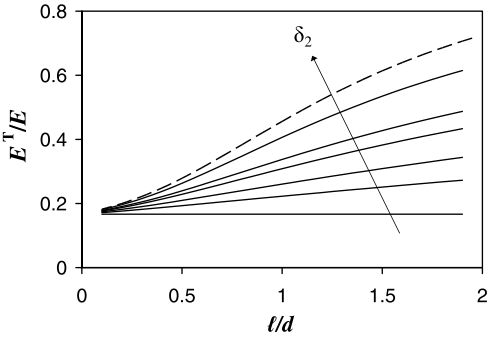


Fig. 6. Normalized tangent modulus vs. $\ell/d$ for $\delta_2 = 0$, 0.5, 1, 2, 3, 10, $\infty$, where the dashed line is for a rigid interface (i.e. $\delta_2 \to \infty$).

$$E^{T}/E = [1 + (E/h)\{1 - \delta_2/[\lambda(1 + \delta_2 \coth \lambda)]\}]^{-1} \tag{43}$$

As can be seen from the above equation that the tangent modulus is dependent on $\lambda = d/\ell$ and $\delta_2$, but independent of $\delta_1$. This dependence is shown in Fig. 6 for different values of $\delta_2$. As can be seen from Fig. 6 that $\delta_2 = 0$ corresponds to a constant tangent modulus independent of $d$ (see Fig. 3c and d) and $\delta_2 \to \infty$ corresponds to a rigid interface where dislocations are not allowed to cross over. Furthermore, it can be seen from Fig. 6 that for very small $d$ (i.e. $\ell/d \to \infty$) and for $\delta_2 \neq 0$, the magnitude of the tangent modulus $E^{T}$ gets closer to the magnitude of the elastic modulus $E$. A physical interpretation of the observed behavior for the case when the interface deforms plastically and hardens is that dislocation movement and nucleation is allowed until dislocations are tangled which results in obstructing further plastic deformation at the interface.

It is noteworthy that the distribution of the plastic strain in Fig. 3a and b for $\delta_1 \neq 0$ and $\delta_2 = 0$ is more diffused and a continuous plastic distribution is seen to form across the entire $d$ resulting in higher yield strengths and constant strain hardening with diminishing size. Whereas for $\delta_1 = 0$ and $\delta_2 \neq 0$ as shown in Fig. 4a and b, the plastic distribution is more localized such that continued deformation is expected to result in the accumulation of geometrically necessary dislocations to accommodate the plastic incompatibility between adjacent interfaces, giving rise to a higher strain hardening.

Moreover, the previous subsection demonstrated that the gradient plasticity allows interfaces to follow their own yield behavior and hence an *interfacial yield stress*, Eq. (42), is present. Particularly, this stress is proportional to the interfacial yield strength, $\gamma$. However, it can be shown by following the same steps for obtaining Eq. (42) that the interfacial yield stress, $\sigma_c$, is independent of the interfacial hardening, $\beta$. This is clearly seen in Fig. 5c and d where the yielding stress is independent of $\ell/d$ such that both the bulk interior and the interface yield at the same time.

From the above results, one concludes that the inclusion of the interfacial hardening, $\beta$, is able to qualitatively describe the strain hardening (i.e. increase in flow stress and tangent modulus), but it cannot predict any strengthening (i.e. increase in the yield strength) with decreasing size. On the other hand, the inclusion of the interfacial yield strength, $\gamma$, is able to qualitatively predict strengthening but without further increasing the strain hardening rate with decreasing size. Therefore, since an increase in the yield strength is usually accompanied by an increase in the hardening rate, which is often seen in experimental results for diminishing sizes (e.g. Huang and Spaepen, 2000; Shrotriya et al., 2003; Haque and Saif, 2003; Espinosa et al., 2004; Uchic et al., 2004; Dimiduk et al., 2005; Greer et al., 2005; Volkert and Lilleodden, 2006; Simons et al., 2006), the combined influence of both $\beta$ and $\gamma$ is discussed next.

### 4.3. The combined influence of the interfacial yield strength and interfacial hardening – Cases (3) and (4)

Here, the combined effect of the interfacial yield strength $\gamma$ (represented by $\delta_1$) and the interfacial hardening $\beta$ (represented by $\delta_2$) is examined. First the interfacial yield condition in Eq. (29) is investigated such that $\delta_1 \neq \delta_2$. Fig. 7a–d shows the plastic strain distribution and the average stress–strain relation for $\delta_1 = 0.45$ and for two values of the interfacial hardening; namely $\delta_2 = 1$ and $\delta_2 = 10$. As expected, Fig. 7c and d shows that both the yield strength and the strain hardening rate increase with decreasing the

characteristic size $d$. This is a desirable behavior since it conforms to the experimental results at the micron and submicron length scales (see Fleck et al., 1994; Huang and Spaepen, 2000; Haque and Saif, 2003; Espinosa et al., 2004). However, it can be seen from Fig. 7c and d that the rate of increase in the yield strength is decreasing as the inter-

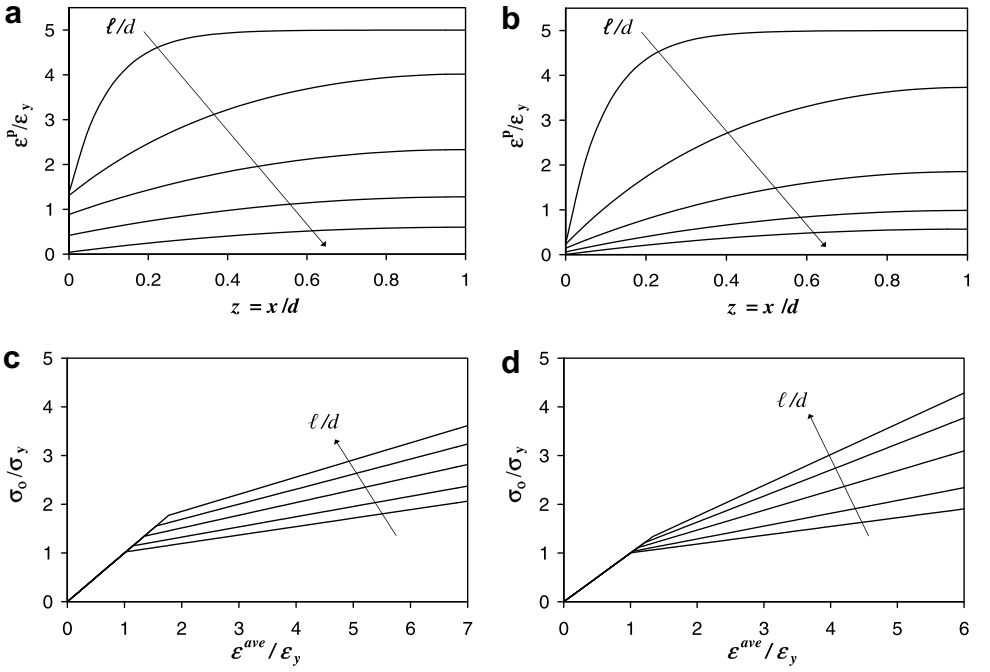


Fig. 7. Size effect due to the combined effect of interfacial yield strength and interfacial hardening. The interfacial yield strength is represented by $\delta_1 = 0.45$. The interfacial hardening is varying according to [(a) and (c)] $\delta_2 = 1$ and [(b) and (d)] $\delta_2 = 10$. (a) and (b) normalized plastic strain distribution along $d$ for $\bar{\sigma}_0 = 2$. (c) and (d) normalized stress–strain relations. Different sizes are represented by $\ell/d = 0.1$, 0.5, 1, 1.5, 2.

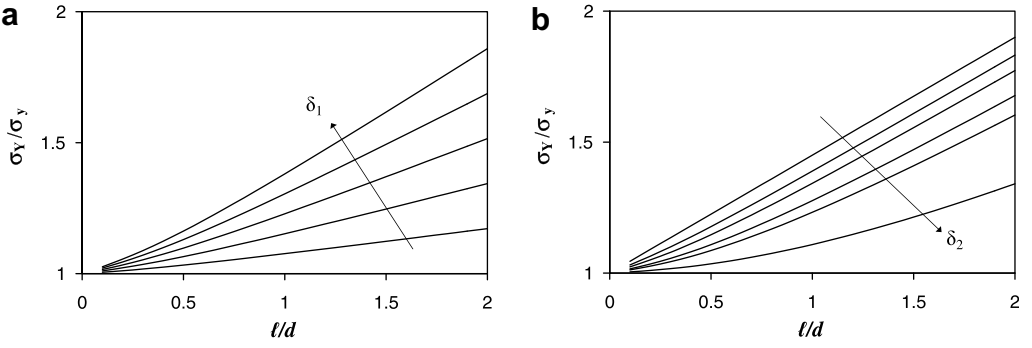


Fig. 8. (a) Normalized yield strength vs. $\ell/d$ for fixed interfacial hardening, $\delta_2 = 1$, and varying interfacial yield strength, $\delta_1 = 0.1$, 0.2, 0.3, 0.4, 0.5. (b) Normalized yield strength vs. $\ell/d$ for fixed interfacial yield strength, $\delta_1 = 0.45$, and varying interfacial hardening, $\delta_2 = 0$, 0.5, 1, 2, 10.

facial hardening (characterized by $\delta_2$) increases. This is undesirable behavior and does not conform to the experimental observations. An expression for the normalized yield strength $\bar{\sigma}_Y$ as a function of both $\delta_1$ and $\delta_2$ can be obtained by following the same steps used in obtaining Eq. (39) such that by integrating Eq. (37) for $z$ and solving for $\bar{\sigma}_0 = \bar{\sigma}_Y$ by setting $(\bar{\varepsilon}^p)^{ave} = 0$ yields:

$$\bar{\sigma}_Y = 1 + \frac{\delta_1}{\lambda + \delta_2(\lambda \coth \lambda - 1)} \tag{44}$$

It can be seen from the above equation that the global yield strength is sensitive to both the interfacial yield strength and the interfacial hardening. Eq. (44) can be plotted versus $\ell/d$ and for different values of the interfacial yield strength, $\delta_1$, and interfacial hardening, $\delta_2$. Fig. 8a shows that the global yield strength increases with increasing $\delta_1$ at fixed $\delta_2 = 1$, but this increase is slightly nonlinear as compared to Eq. (39). Whereas, Fig. 8b shows that the global yield strength decreases with increasing $\delta_2$ at fixed $\delta_1 = 0.45$, which is an undesirable behavior (see Fig. 1) since one expects that by increasing the interfacial hardening, increase in both the yield strength and strain hardening rate should be encountered. A physical interpretation is that the dislocation interaction at the interface increases by increasing interfacial hardening which results in a stiff network of dislocations and increases the resistance to further plastic deformation at the interface such that a stiff interface is obtained.

On the other hand, if one adopts the interfacial yield condition in Eq. (30), which is equivalent to setting $\delta_1 = \delta_2 = \delta = \ell_I/\ell$ in Eqs. (36), (37), (38) and (44), a different behavior is seen when altering $\delta$ as shown in Fig. 9c and d as compared to Fig. 7c and d, while the plastic strain distribution is not affected as shown in Fig. 9a and b compared to Fig. 7a and b. It can be seen from Fig. 9c and d that both the global yield strength and strain hardening rate are increased with decreasing $d$ and increasing $\delta$, which conforms to the experimental results as schematically shown in Fig. 1. This behavior can be clearly seen by setting $\delta_1 = \delta_2 = \delta$ in Eq. (44),

$$\bar{\sigma}_Y = 1 + [\lambda/\delta + \lambda \coth \lambda - 1]^{-1} \tag{45}$$

and plotting $\bar{\sigma}_Y$ versus $\ell/d$ for different values of $\delta$ as shown in Fig. 10 compared to that in Fig. 8b. Therefore, for a stiff or rigid interface, where dislocations are not allowed to penetrate, one can write an expression for the global yield strength by setting $\delta \to \infty$ in Eq. (45) such that

$$\bar{\sigma}_Y = 1 + [\lambda \coth \lambda - 1]^{-1} \tag{46}$$

This equation is shown in Fig. 10 and indicated by the dashed line. Hence, in this case $d$ alone (represented by the ratio $\ell/d$) controls the increase in the yield strength, whereas for compliant and intermediate interfaces both $d$ and $\delta$ determine the yield strength. Moreover, for a rigid interface, strain hardening is controlled by $d$ alone, which can be shown by setting $\delta_2 = \delta \to \infty$ in Eq. (43)

$$E^T/E = [1 + (E/h)\{1 - 1/[\lambda \coth \lambda]\}]^{-1} \tag{47}$$

which is shown in Fig. 6 and indicated by the dashed line. The results in Eqs. (46) and (47) agree very well with the conclusions of Fredriksson and Gudmundson (2005) and Anand et al. (2005) who showed that a rigid interface results in a pronounced increase

in the yield strength and strain hardening with diminishing size. Accordingly, one may accept the use of the interfacial yield condition in Eq. (30) over that in Eq. (29) to model the size effect behavior in micro/nano-systems. The above results also suggest that if the interface is compliant or intermediate in terms of constraining plastic deformation, it determines the yield strength and strain hardening of the specimen. In this case, the interfacial length scale, $\ell_I$, will control the size effects. On the other hand, if the interface is stiff or rigid in terms of constraining plastic deformation, it will not influence the yield strength and strain hardening of the specimen. In this case, the bulk length scale, $\ell$, will control the size effect. This means that size effect is controlled by the weakest link of bulk and interface.

It is noteworthy that the same expression for the interfacial yield stress in Eq. (42) can be obtained for this case of combined interfacial yield and hardening effects such that one finds that $\sigma_c$ is not dependent on the interfacial hardening but primarily dependent on the interfacial yield strength.

The behavior in Figs. 9 and 10 can be interpreted as when the applied stress reach the local yield stress, dislocations are nucleated in the bulk interior and with continued deformation these dislocations get pinned and pile-up at interfaces. Once the applied stress concentration at the tip of leading dislocation reaches the interfacial yield stress, the interface deforms plastically and then deformation transmits across the interface. Once dislocations start transferring across the interface, interfacial hardening is activated which leads to

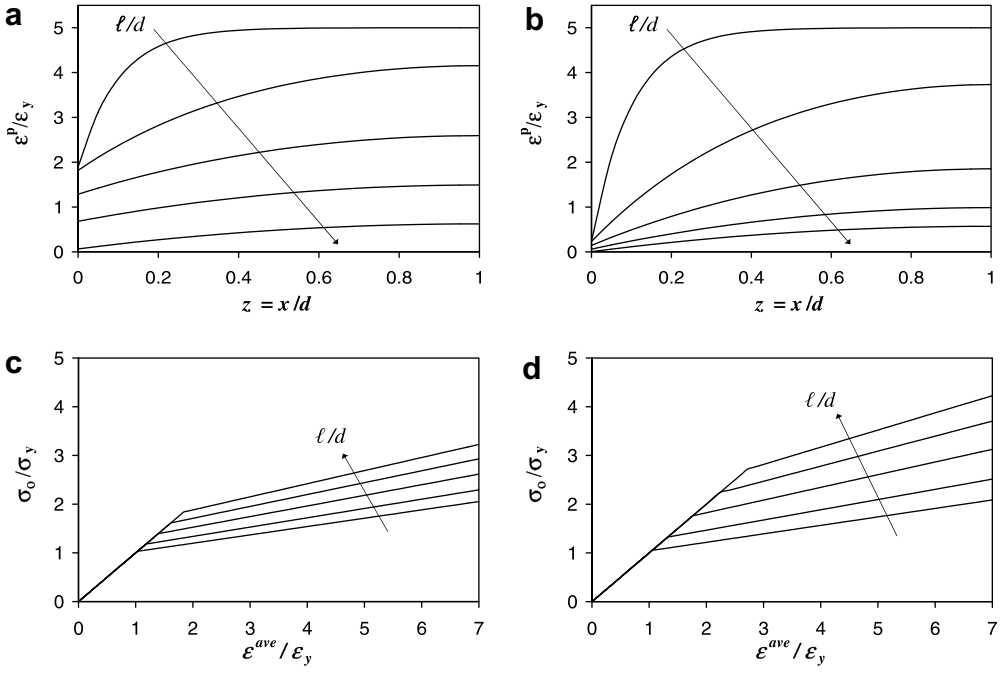


Fig. 9. Size effects due to interfacial yield strength and interfacial hardening for $\delta_1 = \delta_2 = \delta$. Both the interfacial yield strength and hardening is varying simultaneously according to [(a) and (c)] $\delta = 0.45$ and [(b) and (d)] $\delta = 1$. (a) and (b) normalized plastic strain distribution along $d$ for $\bar{\sigma}_0 = 2$. (c) and (d) normalized stress–strain relations. Different sizes are represented by $\ell/d = 0.1, 0.5, 1, 1.5, 2$.

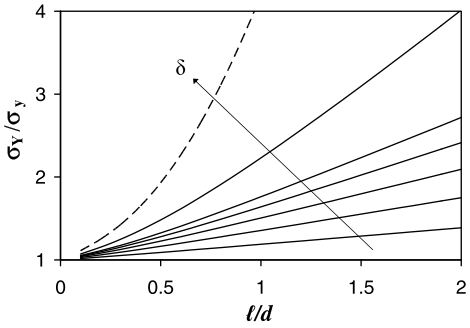


Fig. 10. Normalized yield strength vs. $\ell/d$ for varying simultaneously the interfacial yield strength and hardening and setting $\delta_1 = \delta_2 = \delta = 0.2$, 0.4, 0.6, 0.8, 1, 2, and $\infty$. The dashed line is for a rigid interface (i.e. $\delta \to \infty$).

strengthening of the interface that in turn increases the global yield strength of the material. However, with the increase of interfacial hardening and dislocation transmission and emission at the interface, dislocations interact at the interface and in the bulk interior such that dislocation transmission across the interface is suppressed which increases the rate of strain hardening of the material. The suppression of dislocation transmission across the interface suggests that the interfacial yield strength is recovered and a stiff interface is formed such that both the yield strength and strain hardening are increased with diminishing size.

It can be noted from the plastic strain distributions in Figs. 3, 5, 7 and 9 that due to the constraint placed on the plastic strain, a boundary layer develops through $d$. Interestingly, the thickness of the boundary layer is independent of the applied stress and does not vary with time, but scales with $\ell$ and $\ell_I$.

Moreover, it is noteworthy that the inclusion of interfacial yielding results, according to the notion of Gurtin (e.g. Gurtin, 2003; Gurtin and Needleman, 2005; Anand et al., 2005), in a dissipative hardening effect with strengthening, while the inclusion of the interfacial hardening results in an energetic hardening effect without strengthening. Therefore, both effects should be incorporated in order to qualitatively predict size effect.

## 5. Summary and conclusions

In this paper, the effect of interface properties (yield strength and hardening) on the scale-dependent behavior of small-scale systems is studied within the framework of higher-order gradient plasticity theory. It is shown that the additional microscopic boundary conditions, which are supplemented by the gradient approach, allows one to predict size effects under uniform stressing. This is achieved by relating the microtraction stress at interfaces to an interfacial energy that depends on the plastic strain at the interface. Furthermore, by examining linear and nonlinear expressions for this interfacial energy, it is shown that an interfacial yield condition, besides the nonlocal yield condition for the bulk, can be formulated. This condition governs the emission/transmission of dislocations across the interface and is expressed in terms of the microtraction stress, the interfacial yield strength, the interfacial hardening, and the interfacial length scale. Therefore, two internal length scales are incorporated in the present formalism, one for the bulk, $\ell$, and the other for the interface, $\ell_I$.

It is shown that the higher-order gradient plasticity theory when supplemented by interfacial energy effects, at least for the one-dimensional example presented here, can qualitatively describe many features of the size effect due to GNDs, including the strengthening, the development of boundary layers, and the strain hardening. The qualitative modeling of the strengthening is explained by the interfacial yield strength, whereas the strain hardening is described by accounting for the interfacial hardening effect.

Four different forms for the interfacial energy (or equivalently the interfacial yield condition) in terms of the plastic strain at the interface are examined: (a) a linear one which allows the interface to yield in a perfectly plastic manner without hardening; (b) a quadratic form which allows the interface to harden but yields at the same time as the bulk; (c) a combination of (a) and (b) such that the interfacial yield strength and interfacial hardening can be altered independently; and (d) a combination of (a) and (b) such that the interfacial yield strength and interfacial hardening are both scaled with the interfacial length scale. It is found through (a) that that interfacial yield strength controls the overall yield strength (i.e. onset of plasticity) of the specimen. Moreover, an analytical expression for the *interfacial yield stress* at which interface deforms plastically is derived. This is one of the most interesting features of the present formulation. From this expression, it is concluded that the yield strength of ultra-fine grained materials is controlled by the interfacial strength of the grain boundary. Moreover, it is found through (b) that interfacial hardening controls the increase in the plasticity tangent hardening modulus and in the flow stress with decreasing size. The expression in (c) shows that the interfacial hardening contributes to the global yield strength as well as to the strain hardening rates (i.e. flow stress). However, it is shown that the expression in (c) yields incorrect decrease in the yield strength when increasing the interface stiffness. This is corrected by adapting the expression in (d) which shows that by increasing the interfacial hardening, stiffer interfaces are formed that in turn increases the yield strength of the material due to dislocation networking at the interface which obstructing further emission/transmission of dislocations across the interface. Therefore, it is concluded that the interfacial length scale should scale the effect of both the interfacial yield strength and interfacial hardening. Moreover, one should be careful when choosing a proper form for the interfacial energy such that it should at least qualitatively confirms with the experimental observations of size effect behavior.

It is concluded that the increase in the material's yield strength and strain hardening rates with decreasing size is determined by the weakest link of bulk and interface. If the interface is compliant then the properties of the interface control the yield strength and hardening rates of the material (i.e. controlled by the interfacial length scale $\ell_{\mathrm{I}}$). On the other hand, if the interface is rigid, the yield strength and hardening rates are controlled by the bulk behavior (i.e. controlled by the bulk length scale $\ell$). Therefore, for intermediate interfaces, a competition between those two mechanisms exists.

Interfacial effect is an important aspect for further development of gradient-dependent plasticity that is capable of modeling size effects in micro/nano-systems that are initially subjected to macroscopically uniform stresses or strains. It is shown that the existence of both gradients and interfacial energies contribute to the observed size effects. Moreover, it is emphasized that in the absence of the interfacial energy, the material would support uniform fields and hence the constitutive gradient-dependence would have no influence. Therefore, strain gradients come into play if the boundaries are assumed to constrain

the plastic flow. Therefore, if continuum theories are to be used to predict plastic behavior at the micron or submicron length scales, a higher-order theory with interfacial energies is likely to be required.

Also, it would be interesting to compare the results provided by the present theory and its rate form counterpart obtained in two- or three-dimensional applications. In a forthcoming work, a detailed Finite Element implementation of the proposed model will be presented and used to simulate size effect in small-scale structures under various loading conditions (e.g. bending, torsion, cyclic loading). Moreover, it is interesting to validate the present conclusions by performing detailed discrete dislocation dynamics.

It is noteworthy that several researchers have questioned the ability of strain gradient plasticity theory to explain the observed size effect in nano/micro pillars or columns when subjected to macroscopically homogenous deformation (e.g. Uchic et al., 2004; Dimiduk et al., 2005; Greer et al., 2005). These debates are attributed to the absence of strain gradients in these systems when subjected to uniform straining or stressing. Moreover, it has been argued that this type of size effect is due to dislocation starvation; i.e. the rate at which dislocations multiply is less than that rate at which dislocations escape and annihilate from the pillar surface as the size decreasing to hundreds of nanometers. However, in a recent experimental study by Bei et al. (2007) on the compressive strengths of various sizes of single-crystal micro-pillars of a molybdenum alloy, which are prepared by a new technique that generates much less defects as compared to the use of Focused Ion Beam (FIB), it is shown that dislocation starvation does not occur. Moreover, most of the work regarding dislocation starvation is for single crystals. If there are grain boundaries, then clearly the "easy" loss of dislocations is greatly inhibited. In a forthcoming paper by the author, it will be shown that the surface energy at the free surface of a micro/nano pillar can be used within the proposed framework of higher-order gradient plasticity to describe the observed strong size effect in nano/micro pillars. This can be simply done by applying non-trivial microscopic boundary conditions at the free surfaces in terms of the surface energy such that Eq. (26) can be written as

$$\boldsymbol{m}_{ij} = \boldsymbol{m}_{ij_0} + \frac{\partial \varphi(\boldsymbol{\varepsilon}^{\mathrm{p(I)}})}{\partial \varepsilon_{ij}^{\mathrm{p(I)}}} \tag{48}$$

where $m_{ij_0} = \tau_0 \delta_{ij}$ is the initial surface stress with $\tau_0$ representing the deformation-independent surface tension. Therefore, while the extrinsic applied stresses are relatively uniform during micro-compression, the internal strain gradients may still controlling the size effect response and a higher-order gradient plasticity theory of the present form with surface energy effects could be used to explain the size effect in these experiments.

Finally, more than 50 years of research on grain boundaries has established their impact on the overall strength of materials, yet experimental studies on their yield strength or Young's modulus are rare in the literature. This is because grain boundaries are random networks of interfaces that are only a few nanometers wide and cannot be isolated and characterized by conventional tensile, bending, indentation tools. Therefore, the fundamental understanding on the interfaces in materials will impact grain boundary engineering, an evolving research direction towards optimized materials design. Initial attempts in this direction are of Aifantis et al. (2006).

## References


Abu Al-Rub, R.K., 2007. Prediction of micro- and nano indentation size effect from conical or pyramidal indentation. Mech. Mater. 39, 787–802.

Abu Al-Rub, R.K., Voyiadjis, G.Z., 2004a. Analytical and experimental determination of the material intrinsic length scale of strain gradient plasticity theory from micro- and nano-indentation experiments. Int. J. Plast. 20, 1139–1182.

Abu Al-Rub, R.K., Voyiadjis, G.Z., 2004b. Determination of the material intrinsic length scale of gradient plasticity theory. Int. J. Multiscale Comput. Eng. 3 (3), 50–74.

Abu Al-Rub, R.K., Voyiadjis, G.Z., 2006. A physically based gradient plasticity theory. Int. J. Plast. 22, 654–684.

Abu Al-Rub, R.K., Voyiadjis, G.Z., Bammann, D.J., 2007. A thermodynamic based higher-order gradient theory for size dependent plasticity. Int. J. Solids Struct. 44, 2888–2923.

Acharya, A., Bassani, J.L., 2000. Lattice incompatibility and a gradient theory of crystal plasticity. J. Mech. Phys. Solids 48, 1565–1595.

Aifantis, E.C., 1984. On the microstructural origin of certain inelastic models. J. Eng. Mater. Technol. 106, 326–330.

Aifantis, K.E., Willis, J.R., 2005. The role of interfaces in enhancing the yield strength of composites and polycrystals. J. Mech. Phys. Solids 53, 1047–1070.

Aifantis, K.E., Willis, J.R., 2006. Scale effects induced by strain-gradient plasticity and interfacial resistance in periodic and randomly heterogeneous media. Mech. Mater. 38, 702–716.

Aifantis, K.E., Soer, W.A., De Hosson, J.Th.M., Willis, J.R., 2006. Interfaces within strain gradient plasticity: theory and experiments. Acta Mater. 54, 5077–5085.

Anand, L., Gurtin, M.E., Lele, S.P., Gething, C., 2005. A one-dimensional theory of strain-gradient plasticity: formulation, analysis, numerical results. J. Mech. Phys. Solids 53, 1789–1826.

Asaro, R.J., 1983. Crystal plasticity. J. Appl. Mech. 50, 921–934.

Ashby, M.F., 1970. The deformation of plastically non-homogenous alloys. Philos. Mag. 21, 399–424.

Balint, D., Deshpande, V., Needleman, A., Van der Giessen, E., 2005. A discrete dislocation plasticity analysis of grain-size strengthening. Mater. Sci. Eng. A, 186–190.

Bei, H., Shim, S., George, E.P., Miller, M.K., Herbert, E.G., Pharr, G.M., 2007. Compressive strengths of molybdenum alloy micro-pillars prepared using a new technique. Scripta Mater. 57, 397–400.

Benzerga, A.A., Shaver, N.F., 2006. Scale dependence of mechanical properties of single crystals under uniform deformation. Scripta Mater. 54, 1937–1941.

Biner, S., Morris, J., 2002. A two-dimensional discrete dislocation simulation of the effect of grain size on strengthening behaviour. Model. Simul. Mater. Sci. Eng. 10, 617–635.

Balint, D.S., Deshpande, V.S., Needleman, A., Van der Giessen, E., 2007. Discrete dislocation plasticity analysis of the grain size dependence of the flow strength of polycrystals. Int. J. Plast. doi:10.1016/j.ijplas.2007.08.005.

Borg, U., 2007. A strain gradient crystal plasticity analysis of grain size effects in polycrystals. Eur. J. Mech. A/Solids 26 (2007), 313–324.

Clayton, J.D., McDowell, D.L., Bammann, D.J., 2006. Modeling dislocations and disclinations with finite micropolar elastoplasticity. Int. J. Plast. 22, 210–256.

DeGuzman, M.S., Neubauer, G., Flinn, P., Nix, W.D., 1993. The role of indentation depth on the measured hardness of materials. Mater. Res. Symp. Proc. 308, 613–618.

Dimiduk, D.M., Uchic, M.D., Parthasarathy, T.A., 2005. Size-affected single-slip behavior of pure nickel microcrystals. Acta Mater. 53, 4065–4077.

Edelen, D.G.B., Laws, N., 1971. On the thermodynamics of systems with nonlocality. Arch. Ration. Mech. An. 43, 24–35.

Elmustafa, A.A., Stone, D.S., 2002. Indentation size effect in polycrystalline F.C.C metals. Acta Mater. 50, 3641–3650.

Eringen, A.C., Edelen, D.G.B., 1972. On non-local elasticity. Int. J. Eng. Sci. 10, 233–248.

Espinosa, H.D., Prorok, B.C., Peng, B., 2004. Plasticity size effects in free-standing submicron polycrystalline FCC films subjected to pure tension. J. Mech. Phys. Solids 52, 667–689.

Espinosa, H.D., Panico, M., Berbenni, S., Schwarz, K.W., 2006. Discrete dislocation dynamics simulations to interpret plasticity size and surface effects in freestanding FCC thin films. Int. J. Plast. 22, 2091–2117.

Evers, L., Brekelmans, W., Geers, M., 2004. Scale dependent crystal plasticity framework with dislocation density and grain boundary effects. Int. J. Solids Struct. 41, 5209–5230.

Fleck, N.A., Muller, G.M., Ashby, M.F., Hutchinson, J.W., 1994. Strain gradient plasticity: theory and experiment. Acta Metall. Mater. 42, 475–487.
Fredriksson, P., Gudmundson, P., 2005. Size-dependent yield strength of thin films. Int. J. Plast. 21, 1834–1854.
Fredriksson, P., Gudmundson, P., 2007. Modelling of the interface between a thin film and a substrate within a strain gradient plasticity framework. J. Mech. Phys. Solids 55, 939–955.
Gao, H., Huang, Y., Nix, W.D., Hutchinson, J.W., 1999. Mechanism-based strain gradient plasticity – I. Theor. J. Mech. Phys. Solids 47, 1239–1263.
Gao, H., Huang, Y., 2001. Taylor-based nonlocal theory of plasticity. Int. J. Solids Struct. 38, 2615–2637.
Greer, J.R., Oliver, W.C., Nix, W.D., 2005. Size dependence of mechanical properties of gold at the micron scale in the absence of strain gradients. Acta Mater. 53, 1821–1830.
Gurtin, M.E., 2000. On the plasticity of single crystals: free energy, microforces, plastic-strain gradients. J. Mech. Phys. Solids 48, 989–1036.
Gurtin, M.E., 2002. A gradient theory of single-crystal viscoplasticity that accounts for geometrically necessary dislocations. J. Mech. Phys. Solids 50 (1), 5–32.
Gurtin, M.E., 2003. On a framework for small-deformation viscoplasticity: free energy, microforces, strain gradients. Int. J. Plast. 19, 47–90.
Gurtin, M.E., Murdoch, A.I., 1978. Surface stress in solids. Int. J. Solids Struct. 14, 431–440.
Gurtin, M.E., Needleman, A., 2005. Boundary conditions for small deformation, single crystal plasticity that account for the Burgers vector. J. Mech. Phys. Solids 53, 1–31.
Gudmundson, P., 2004. A unified treatment of strain gradient plasticity. J. Mech. Phys. Solids 52, 1379–1406.
Haque, M.A., Saif, M.T.A., 2003. Strain gradient effect in nanoscale thin films. Acta Mater. 51, 3053–3061.
Hirth, J.P., 1972. Influence of grain boundaries on mechanical properties. Metall. Trans. 3, 3047–3067.
Huang, H., Spaepen, F., 2000. Tensile testing of free-standing Cu, Ag and Al thin films and Ag/Cu multilayers. Acta Mater. 48, 3261–3269.
Kiser, M.T., Zok, F.W., Wilkinson, D.S., 1996. Plastic flow and fracture of a particulate metal matrix composite. Acta Mater. 44, 3465–3476.
Kumar, K., Van Swygenhoven, H., Suresh, S., 2003. Mechanical behavior of nanocrystalline metals and alloys. Acta Mater. 51, 5743–5774.
Lefebvre, S., Devincre, B., Hoc, T., 2007. Yield stress strengthening in ultrafine-grained metals: a two-dimensional simulation of dislocation dynamics. J. Mech. Phys. Solids 55, 788–802.
Lim, Y.Y., Chaudhri, Y.Y., 1999. The effect of the indenter load on the nanohardness of ductile metals: an experimental study of polycrystalline work-hardened and annealed oxygen-free copper. Philos. Mag. A 79 (12), 2979–3000.
Lloyd, D.J., 1994. Particle reinforced aluminum and magnesium matrix composites. Int. Mater. Rev. 39, 1–23.
Ma, Q., Clarke, D.R., 1995. Size dependent hardness in silver single crystals. J. Mater. Res. 10, 853–863.
McElhaney, K.W., Valssak, J.J., Nix, W.D., 1998. Determination of indenter tip geometry and indentation contact area for depth sensing indentation experiments. J. Mater. Res. 13, 1300–1306.
Nan, C.-W., Clarke, D.R., 1996. The influence of particle size and particle fracture on the elastic/plastic deformation of metal matrix composites. Acta Mater. 44, 3801–3811.
Nicola, L., Van der Giessen, E., Needleman, A., 2003. Discrete dislocation analysis of size effects in single crystal thin films. J. Appl. Phys. 93, 5920–5928.
Nix, W.D., 1989. Mechanical properties of thin films. Metall. Trans. A 20, 2217–2245.
Nix, W.D., Gao, H., 1998. Indentation size effects in crystalline materials: a law for strain gradient plasticity. J. Mech. Phys. Solids 46, 411–425.
Prager, W., 1956. A new method of analyzing stresses and strains in work-hardening plastic solids. J. Appl. Mech., ASME 23, 493–496.
Polizzotto, C., Borino, G., 1998. A thermodynamics-based formulation of gradient-dependent plasticity. Eur. J. Mech. A/Solids 17, 741–761.
Polizzotto, C., 2003. Unified thermodynamic framework-for nonlocal/gradient continuum theories. Eur. J. Mech. A/Solids 22, 651–668.
Poole, W.J., Ashby, M.F., Fleck, N.A., 1996. Micro-hardness of annealed and work-hardened copper polycrystals. Scripta Mater. 34, 559–564.
Read, W.T., Shockley, W., 1950. Dislocation models of crystal grain boundaries. Phys. Rev. 78, 275–289.
Rhee, M., Hirth, J.P., Zbib, H.M., 1994. A superdislocation model for the strengthening of metal matrix composites and the initiation and propagation of shear bands. Acta Metall. Mater. 42, 2645–2655.
Scheidler, M., Wright, T.W., 2001. A continuum framework for finite viscoplasticity. Int. J. Plast. 17, 1033–1085.

Shrotriya, P., Allameh, S.M., Lou, J., Buchheit, T., Soboyejo, W.O., 2003. On the measurement of the plasticity length scale parameter in LIGA nickel foils. Mech. Mater. 35, 233–243.

Simons, G., Weippert, Ch., Dual, J., Villain, J., 2006. Size effects in tensile testing of thin cold rolled and annealed Cu foils. Mater. Sci. Eng. A 416, 290–299.

Stelmashenko, N.A., Walls, M.G., Brown, L.M., Milman, Y.V., 1993. Microindentation on W and Mo oriented single crystals: an STM study. Acta Metall. Mater. 41, 2855–2865.

Stolken, J.S., Evans, A.G., 1998. A microbend test method for measuring the plasticity length-scale. Acta Mater. 46, 5109–5115.

Swadener, J.G., George, E.P., Pharr, G.M., 2002. The correlation of the indentation size effect measured with indenters of various shapes. J. Mech. Phys. Solids 50, 681–694.

Uchic, M.D., Dimiduk, D.M., Florando, J.N., Nix, W.D., 2004. Sample dimensions influence strength and crystal plasticity. Science 305, 986–989.

Venkatraman, R., Bravman, J.C., 1992. Separation of film thickness and grain-boundary strengthening effects in Al thin-films on Si. J. Mater. Res. 7, 2040–2048.

Volkert, C.A., Lilleodden, E.T., 2006. Size effects in the deformation of sub-micron Au columns. Philos. Mag. 86, 5567–5579.

von Blanckenhagen, B., Arzt, E., Gumbsch, P., 2004. Discrete dislocation simulation of plastic deformation in metal thin films. Acta Mater. 52, 773–784.

Voyiadjis, G.Z., Abu Al-Rub, R.K., 2005. Gradient plasticity theory with a variable length scale parameter. Int. J. Solids Struct. 42, 3998–4029.

Voyiadjis, G.Z., Abu Al-Rub, R.K., Palazotto, A.N., 2004. Thermodynamic formulations for non-local coupling of viscoplasticity and anisotropic viscodamage for dynamic localization problems using gradient theory. Int. J. Plast. 20, 981–1038.

Zhu, H.T., Zbib, H.M., 1995. Flow strength and size effect of an Al–Si–Mg composite model system under multiaxial loading. Scripta Metall. Mater. 32, 1895–1902.

Zikry, M.A., Kao, M., 1996. Inelastic microstructural failure mechanisms in crystalline materials with high angle grain boundaries. J. Mech. Phys. Solids 44, 1765–1798.